



Hydrogen Peroxide Gas Sensors

Aroutiounian VM*

Yerevan State University, Armenia

***Corresponding author:** Aroutiounian VM, Yerevan State University, Armenia, Email: kisahar@ysu.am

Review Article

Volume 5 Issue 2

Received Date: October 25, 2021

Published Date: November 22, 2021

DOI: 10.23880/psbj-16000194

Abstract

The results of studies of many types of semiconductor H_2O_2 sensors are discussed in this review of 195 articles about hydrogen peroxide. The properties of electrochemical detectors, sensors based on organic and inorganic materials, graphene, and nano-sensors are analyzed. Optical and fluorescent sensors, detectors made of porous materials, quantum dots, fibers, and spheres are briefly discussed. The results of our studies in the YSU of hydrogen peroxide sensors made from solid solutions of carbon nanotubes with semiconducting metal oxides are also presented in the review. The fundamentals of the manufacture of biomarkers of respiration containing hydrogen peroxide vapors, which make it possible to judge the degree of a person's illness with various respiratory diseases (asthma, lung cancer, etc.), are discussed.

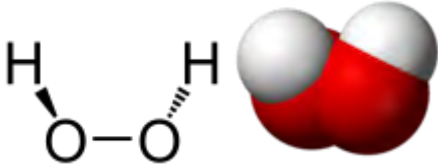
Keywords: Hydrogen Peroxide; Gas Sensors; Organic Materials

Introduction

The determination of trace amounts of hydrogen peroxide is important in environmental, medical, pharmaceutical, and biological fields as well as in the food and textile industry due to a wide spectrum of antibacterial properties, low toxicity, and ecological purity. It is necessary to determine the concentration of hydrogen peroxide H_2O_2 , not only in

chemical and industrial processes (for example, disinfection, waste-water treatment), but also as an intermediate product of an enzyme reaction in biochemical processes (for example, glucose determination). Therefore, an H_2O_2 sensor can be also used as an intermediate transducer for other biosensors.

Properties of H_2O_2 are collected on Internet in Table 1.

Hydrogen peroxide	
	
Properties	
Chemical formula	H_2O_2
Molar mass	34.0147 g/mol
Appearance	Very light blue color; colorless in solution

Odor	slightly sharp
Density	1.11 g/cm ³ (20 °C, 30% (w/w) solution) [1] 1.450 g/cm ³ (20 °C, pure)
Melting point	-0.43 °C (31.23 °F; 272.72 K)
Boiling point	150.2 °C (302.4 °F; 423.3 K) (decomposes)
Solubility	soluble in ether, alcohol insoluble in petroleum ether
Magnetic susceptibility (χ)	$-17.7 \cdot 10^{-6} \text{ cm}^3/\text{mol}$
Refractive index (n_D)	1.4061
Dipole moment	2.26 D

Table 1: Properties of H₂O₂.

Pure H₂O₂ at large concentrations is explosive under certain conditions (for example, in the presence of transition metals). Therefore, concentrated solutions of H₂O₂ can cause burns in the case of contact with skin, mucous membranes, and respiratory tract. H₂O₂ is subsumed under the category of matters those are dangerous for a man with a certain maximum permissible concentrations. Therefore, the development of sensors for the determination of H₂O₂ concentration in the environment is important and attracts the interest of chemists, physicians, industrial engineers, etc. H₂O₂ stable sensors can be used in various fields of the industry and analytical chemistry, for environmental control, in clinical diagnostic. In biology and physiology, H₂O₂ has been recognized as a gesturing molecule for precise and prompt determination of oxidative stress that can be associated with different kinds of chronic diseases such as Alzheimer's, atherosclerosis, lungs injury, cardiovascular diseases, parasitic infections, diabetes, cancer and so on. It is not only a byproduct of numerous oxidases in various biological functions but also a requisite mediator in biomedical, pharmaceutical, food, and environmental analysis. In living systems, its massive accumulation is detrimental for the normal growth of cells and is engendered by the oxidative mitochondrial functions, incomplete reduction of oxygen, and metabolic reactions occurring in live cells. It is noteworthy that H₂O₂ and other reactive oxygen species play a critical role in proliferation, physiological intracellular signaling transduction, straddling development, abiotic anxiety influences, response to lethal attacks, relocation, and distinction of healthy cells [1]. Nevertheless, the excessive production of H₂O₂ in cellular environments is extremely pathogenic to living organisms. Therefore, the determination of the exact level of H₂O₂ paves the way for understanding the pathological, physiological and biomedical role of H₂O₂.

Several techniques have been developed for a determination of H₂O₂ such as spectrophotometry, electrochemical and fluorimetric detection, liquid chromatography, electroanalytical and optical interferometry [2-7]. These techniques are complex, expensive and time consuming.

Electrochemical Sensors for Detection of H₂O₂

A large range of materials such as ferric hexacyanoferrate (Prussian blue) and other metal hexacyanoferrates, metal ophthalocyanines, and metalloporphyrins has been employed for the manufacture of hydrogen peroxide sensors. The advantages of these sensors are simplicity of manufacturing, good response, and capability of control in real time. The possibility for improvement of analytical performances for nanostructuring of Prussian blue (PB) has been reported in Puganova EA [8]. It is possible to make by electrodeposition of nanostructured PB films. Analytical performances of the resulting PB-based nanoelectrode arrays have been studied in course of H₂O₂ detection. The value of sensitivity for sensors was 0.2 AM⁻¹ cm⁻², which is more than for electrodes modified by PB electrodeposited through liquid crystal template. The detection limit was 10⁻⁸ M and a linear calibration range was extending over six orders of magnitude of H₂O₂ concentrations, which are the most advantageous analytical performances in hydrogen peroxide electroanalysis.

In recent years, nanotechnology progress is promoted advances in the field of manufacturing of the H₂O₂ electrochemical sensors.

Hydrogen Peroxide Sensors using Organic Materials

The possibilities of monitoring of vapor phase hydrogen peroxide (VPHPO) decontamination process were investigated by the group headed by Kačer P [9-13]. Polymer matrix-based methylene blue sensors based on their spectra changing in VPHPO were developed. The chemiresistive films made from organic p-type semiconducting phthalocyanines metalized with elements of p-, d-, and f-blocks were sensitive to H₂O₂ vapors [14].

A novel nonenzymatic H₂O₂ sensor has been fabricated and investigated in paper Zhang T [15]. By dispersing copper

nanoparticles onto polypyrrole (PPy) nanowires by cyclic voltammetry (CV) to form PPy-copper nanocomposites on gold electrodes. It was proved [15] that the PPy-copper nanocomposite showed excellent catalytic activity for the reduction of H_2O_2 . The sensor showed a linear response to hydrogen peroxide in the concentration range between 7.0×10^{-6} and 4.3×10^{-3} mol L^{-1} with high sensitivity, and a detection limit of 2.3×10^{-6} mol L^{-1} . Experiment results also showed that the sensor had good stability. A disposable amperometric biosensor for commercial use to detect hydrogen peroxide has been developed in Benedet J [16]. The sensor is based on screen-printed carbon paste electrodes modified by electropolymerization of pyrrole with horseradish peroxidase entrapped. The facture techniques of fabricating the enzyme electrodes are suitable for mass production and quality control. The biosensor shows a linear amperometric response to H_2O_2 from 0.1 to 2.0 mM, with a sensitivity of $33.24 \mu A \text{ mM}^{-1} \text{ cm}^{-2}$. Different operational parameters of electropolymerization are evaluated and optimized.

The preparation of an optical test strip for quantitative assay of H_2O_2 in a aqueous solution was carried out in Naik AN, et al. [17]. Silver nanoparticles (AgNPs) with good optical quality are synthesized here by in-situ reduction of silver ions in the Nafion-117 membrane. The nanocomposite membrane exhibits a narrow Localized Surface Plasmon Resonance (LSPR) band at 413 nm. The extent of decrease in intensity of the LSPR band in presence of H_2O_2 solution gives a quantitative estimate of H_2O_2 concentration. The detector showed a good analytical response towards H_2O_2 detection at pH 7 over a wide concentration range. The detection limit has been calculated to be 2.6×10^{-8} mol L^{-1} , which is lower than the conventional enzyme-based biosensors. It is shown in Yanzi Wu, et al. [18] that the absorbance of oxidized tetramethylbenzidine at 652 nm is linearly correlated with the concentration of H_2O_2 . H_2O_2 acts as a powerful oxidizing agent, so it could be applied in many organic compound synthesis reactions [19].

Hydrogen Peroxide Sensors Made from Non-Organic Materials

H_2O_2 sensors made recently on perovskite [20], gold-decorated pyramidal silicon [21], haematite photoanodes [22], paper Ragavan KV, Busa LSA [23,24], spinach ferredoxin on Au electrode [25], montmorillonite-supported copper sulfide nanocomposites [26], europium functionalized inorganic hybrid material [27]. Other materials are used like Ti_3C_2Tx (MXene)/Pt nanoparticles-modified glassy carbon electrode for H_2O_2 [28], pheochromocytoma Cells Based on Pt-Au Bimetallic Nanoparticles [29]. Microwave-assisted synthesis of PtAu@C based bimetallic nanocatalysts for non-enzymatic H_2O_2 sensor was carried out in Sahin OG [30]. A

simple and sensitive $Ce(OH)CO_3 / H_2O_2 / TMB$ reaction system was used for the colorimetric determination of H_2O_2 and glucose [31]. FePt-Au ternary metallic nanoparticles with the enhanced peroxidase-like activity were used for ultrafast colorimetric detection of H_2O_2 [32].

A glassy carbon and indium tin oxide (ITO) electrodes have been modified in Thiagarajan S [33] with the nano TiO_2 -Au-KI film by the adsorption of TiO_2 nanoparticles on the electrodes followed by the electrochemical depositions of nano Au and KI film. Further the nano TiO_2 -Au-KI film modified ITO was examined. From the microscopic results, the adsorbed nano TiO_2 particles size was found in the range of 70–100 nm. Here the electrochemical depositions of nano Au were formed as a flower shape were in the size range of 230 nm to 1 μm . The electrochemical behavior of nano TiO_2 -Au-KI film has been examined in different pH solutions. The linear range of detection for H_2O_2 oxidation using nano TiO_2 -Au-KI film was found as 1×10^{-5} to 1×10^{-4} M and 1×10^{-9} to 1×10^{-7} M in CV and differential pulse voltammetry (DPV) techniques. Differential pulse voltammograms of nano TiO_2 -Au-KI film are shown in Figure 1. It shows the DPVs of nano TiO_2 -Au-KI film (pH 7 PBS) for the different concentrations of H_2O_2 . Here the DPVs were recorded by sweeping the potentials in the range of 0–0.9V at a pulse amplitude of 50 mV, and a scan rate at 50 mVs^{-1} . Here the DPVs were recorded in the concentration range of 1×10^{-9} to 1×10^{-7} M H_2O_2 , respectively. Curve a–g in Figure 1 shows the well-defined and stable anodic peak current curves for H_2O_2 oxidation. These anodic DPV curves confirm the H_2O_2 oxidation process on the TiO_2 -Au-KI film modified GCE. Further the oxidation peak currents of H_2O_2 increase linearly with the increasing concentration of H_2O_2 , respectively.

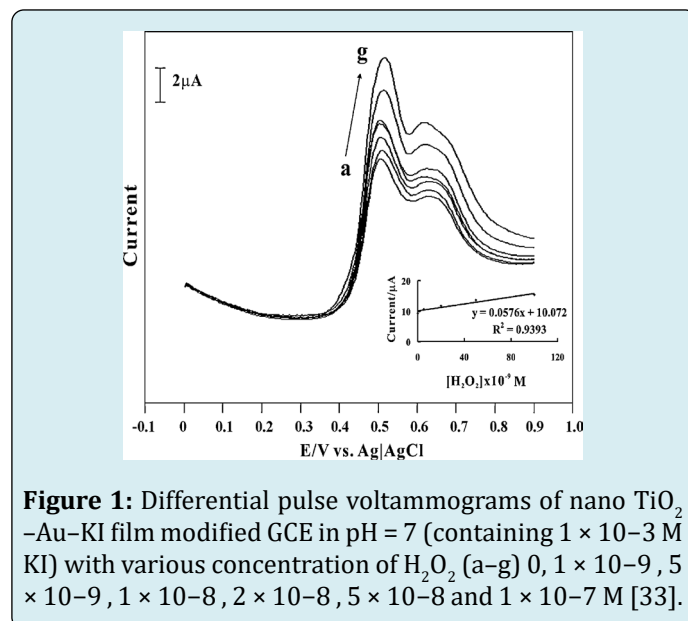


Figure 1: Differential pulse voltammograms of nano TiO_2 -Au-KI film modified GCE in pH = 7 (containing 1×10^{-3} M KI) with various concentration of H_2O_2 (a–g) 0, 1×10^{-9} , 5×10^{-9} , 1×10^{-8} , 2×10^{-8} , 5×10^{-8} and 1×10^{-7} M [33].

The inset of Figure 1 shows the current vs. concentration plot for the electrocatalytic oxidation of H_2O_2 . The above results show that the nano TiO_2 -Au-KI film modified GCE is effective for the electrocatalytic oxidation of H_2O_2 in the nanomolar concentration range by using DPV techniques. The practical applications of nano TiO_2 -Au-KI film were evaluated by analyzing the real samples such as antiseptic and contact lens cleaner solutions containing H_2O_2 .

Structurally integrated metal oxide intercalated layered double hydroxide (LDH) nanospheres (NSs) hybrid material has been of considerable current interest [34]. A new type of MnAl LDH wrapped CuO (CuO@MnAl LDHs) NSs by anchoring CuO nanoparticles (NPs) with MnAl LDHs via a facile co-precipitation and hydrothermal approach was reported. Its practical application as a high-efficient electrocatalyst towards H_2O_2 reduction for biological application was explored. The integration of n-type spinel of CuO and p-type semiconductive channels of MnAl LDHs can accelerate electron transfer at the breakdown voltage of p-n junction. Owing to the synergistic effect of the high surface area of CuO NPs, superb intercalation features of semiconductive MnAl LDHs for encapsulating NSs, and their intrinsic p-n junction characteristics, CuO@MnAl NSs have exhibited excellent electro-catalytic activity towards the reduction of H_2O_2 . When implemented in the electrochemical sensor system, the CuO@MnAl NSs modified electrode displays high nonenzymatic sensing performances towards H_2O_2 , detection limit, good selectivity, and long term stability.

Hydrogen peroxide sensors were manufactured based on different nanocomposites. Among them are Fe_3O_4 - Fe_2O_3 [35], chitosan-coated Fe_3O_4 [36], Au/ Co_3O_4 - $CeOx$ [37], $CuWO_4$ [38], Cu_2O nanowire arrays on copper [39], TaOx-based material in W/ Al_2O_3 /TaOx/TiN structure [40].

Nanosensors for Electrochemical Detection of H_2O_2

The main problem in sensors today is developing new semiconductor gas sensors working at or nearby room temperature of work body (practically without pre-heating it) and use of small-size metal oxides sensors functionalized (decorated) with different impurities, metal coatings or nanotubes, an effective way to increase the specific surface area and conductivity and, as a result, to exploit further advantages for nanoscale sensor applications. We shortly reported in Aroutiounian VM [41] the results of investigations of zero dimensional; one-dimensional nanorods and nanowires, two dimensional nanosheets and films; three-dimensional porous nanostructures; three-dimensional nanostructures functionalized (decorated) with nanotubes. We focused our attention on several gases as ethanol (C_2H_5OH) and acetone (CH_3COCH_3) gases. We just

mention below dimensional effects in small-size sensors (so called nano-sensors) for the detection of H_2O_2 gas. Iron oxide nanorods array for electrochemical detection of H_2O_2 are reported in Lin CY, Li X [42,43], and molybdenum disulfide nanosheets supported Au-Pd bimetallic nanoparticles are proposed for non-enzymatic electrochemical sensing of hydrogen peroxide, glucose, and cancer cells detection.

Hollow-sphere Co_3O_4 nanoparticles were successfully synthesized [44-52]. The resulting Co_3O_4 hollow sphere was exploited as an electrocatalyst for sensitive H_2O_2 detection in an alkaline medium. The Co_3O_4 hollow sphere modified glassy carbon electrode exhibited a fast response time (within 3s), a high sensitivity of $120.55 \mu A/mM$ ($959.79 \text{ mA}\cdot\text{mM}^{-1}\cdot\text{cm}^{-1}$), a broad linear range from 0.4 mM to 2.2 mM, a detection limit of 0.105 mM ($S/N=3$), and good stability and selectivity, suggesting its excellent performance towards H_2O_2 detection [45].

A rapid, reproducible, cost-effective approach for the detection of H_2O_2 has been developed in Shan G, et al. [53] based on the change of localized surface plasmon resonance (LSPR) peak of Au nanorods (NRs). A method for detecting the concentration of H_2O_2 based on the change of LSPR of Au NRs was developed. H_2O_2 can etch Au NRs due to higher standard redox potential. The absorption spectra showed that various ratio of LSPR peaks is proportional to the concentration of H_2O_2 , which suggested that Au NRs can potentially serve as a new sensor for the detection of H_2O_2 .

Graphene H_2O_2 Sensors

Since the discovery of graphene, substantial interest has been aroused to develop graphene gas sensors [54]. In high-quality single-crystalline graphene sheets, the surface-to-bulk ratio reaches 100%, and structural imperfections can be eliminated. When gaseous molecules are adsorbed on graphene, the physical adsorption and ensuing desorption are reversible and this process does not cause structural distortion and property degradation. The general working principle of a graphene sensor is when graphene is originally p-type doped, transferring electrons to graphene will reduce graphene's electrical conductivity, while transferring electrons from graphene to molecules will increase graphene's electrical conductivity; when graphene is originally n-type doped (electron-rich), the outcomes discussed above will be reversed.

It is very promising to use heterosensors made from graphene together with other materials. We will mainly discuss below the use of different heterostructures with graphene for H_2O_2 gas detection. Some new versions of such sensors are discussed recently [55-69]. A new electrocatalyst MnO_2 /graphene oxide hybrid nanostructure was synthesized

for the detection of H_2O_2 [70]. The MnO_2 /graphene oxide-based electrodes showed high electrochemical activity for the detection of H_2O_2 in an alkaline medium. The GO/ MnO_2 electrode presents high sensitivity, low potential and long-term stability towards the detection of H_2O_2 . The amperometric response of the graphene oxide/ MnO_2 electrode to H_2O_2 is shown in Figure 2.

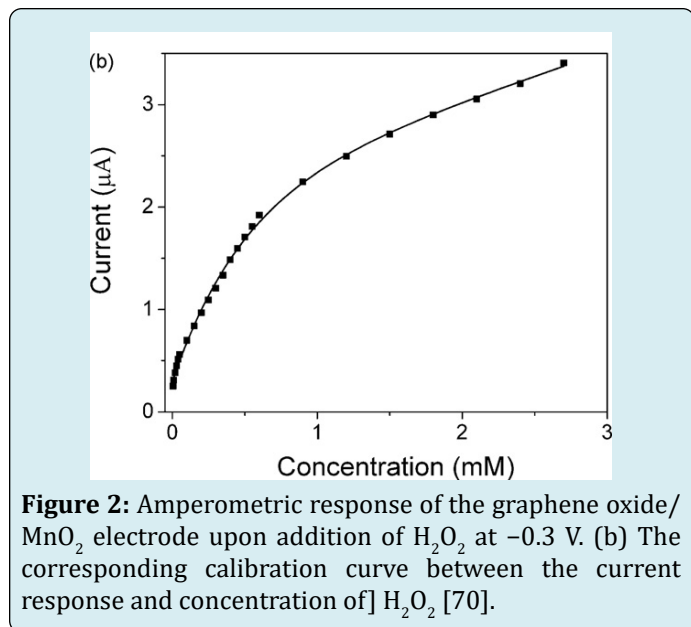


Figure 2: Amperometric response of the graphene oxide/ MnO_2 electrode upon addition of H_2O_2 at -0.3 V. (b) The corresponding calibration curve between the current response and concentration of H_2O_2 [70].

The preparation of NiO/graphene (NiO/GR) nanocomposite for the determination of H_2O_2 was reported in Yu Z, et al. [71]. The electrocatalytic behaviors towards H_2O_2 are investigated by cyclic voltammetry and chronoamperometry in alkaline aqueous solution. High electrocatalytic activity toward the oxidation of H_2O_2 was observed with a detection limit of $0.7664 \mu\text{M}$, high sensitivity of $5.91 \mu\text{A} \text{mM}^{-1} \text{cm}^{-2}$, a wide linear range of 0.25 – 4.75 mM.

A novel nonenzymatic, amperometric sensor for H_2O_2 was developed in Palanisamy S [72] based on an electrochemically prepared reduced graphene oxide (rGO)/zinc oxide (ZnO) composite. RGO/ZnO composite was fabricated on a glassy carbon electrode (GCE) by a green route based on simultaneous electrodeposition of ZnO and electrochemical reduction of graphene oxide (RGO). The electrochemical performance of the rGO/ZnO composite modified GCE was studied by amperometric technique, and the resulting electrode displays excellent performance towards H_2O_2 at -0.38 V in the linear response range from 0.02 to 22.48 mM, with a correlation coefficient of 0.9951 and a short response time (<5 s). The proposed sensor also has good operational and storage stability with appreciable anti-interfering ability.

Let us continue short description of H_2O_2 sensors using

graphene and graphene oxide. The catalytic activity of N-doped graphene toward a peroxidase substrate oxidation in the presence of H_2O_2 is presented in Pogacean F, et al. [73]. In addition, the activity was compared with that of metallic nanoparticles decorated-graphene, achieved either by catalytic chemical vapor deposition with induction heating or by chemical reduction of graphene oxide (rGO). From all investigated graphene-based nanomaterials, the highest activity was exhibited by N-doped graphene and gold nanoparticles supported on chemically reduced graphene oxide. Doping the graphene surface with nitrogen atoms led to a nanomaterial with a better affinity toward H_2O_2 compared to the natural enzyme. Additionally, the systematic study of the catalytic activity for a variety of graphene-based nanomaterials offered important findings for designing new nanomaterials with peroxidase-like activity. The sensing applications presented here are offering a useful comparison of the peroxidase-like ability of a large variety of graphene-based nanomaterials. The results are showing that the oxidation of benzidine derivatives in the presence of H_2O_2 by graphene nanocomposites is mainly due to the known catalytic activity of the superficial metallic nanoparticles and/or the residual functional groups existing in the chemically obtained graphene-based composites. Moreover, in comparison with natural enzymes, doping the graphene surface with nitrogen atoms (N-Gr) led to the formation of a promising platform for building new enzyme mimic nanomaterials.

Graphene oxide nanoribbons (GONRs) were synthesized in the work Zhi-Liang Wu, et al. [74] via the longitudinal unzipping of multi-walled carbon nanotubes (MWCNTs) nanoparticles with the aid of strong oxidants. The MnO_2 /reduced graphene oxide nanoribbons (MnO_2 /rGO NRs) composites were fabricated by means of a reproducible and single-step hydrothermal co-reduction of KMnO_4 and GONRs. MnO_2 /rGONRs exhibited high electrochemical response toward H_2O_2 .

The developed nonenzymatic electrochemical sensor exhibited a well-defined amperometric response towards H_2O_2 in a wide linear range of 0.25 – 2245 M (see Figure 3), and a detection.

Au nanoparticles and reduced graphene oxide (rGO) co-modified TiO_2 nanotube arrays (TNTs) were prepared in Huang S, et al. [75] by the electro-deposition technology for detecting H_2O_2 , O_2 , and NO. A highly ordered TiO_2 nanotube was synthesized based on the anodic oxidation method, and Au nanoparticles in reduced graphene oxide were electro-deposited on the membrane to fabricate an electrochemical electrode. The established Au/rGO/TNTs electrode is as a novel electrode system for H_2O_2 detection with a quick response H_2O_2 at -0.3 V with high sensitivity (1011.35 mA

$\text{M}^{-1}\text{cm}^{-2}$), wide linear range (0.01–22.3 mM), low detection limit (0.006 mM), good stability and enzyme-like selectivity. In addition, it holds great promise to the preparation of electrochemical sensing and biosensing platform based on the electrocatalytic behaviors of different kinds of important electroactive compounds such as dissolved O_2 and nitrite ions. As is demonstrated in Aroutiounian V [54], rGO sheets are uniquely advantageous to serve as conductive support to uniformly anchor Au nanoparticles with well-defined size and shapes, in which the agglomeration of Au nanoparticles in the common electrode is avoided. Based on the particular architecture and novel performance, the Au/rGO/TNTs hybrid could be an extremely promising candidate applicable for a wide range of electrochemical sensing and biosensing applications.

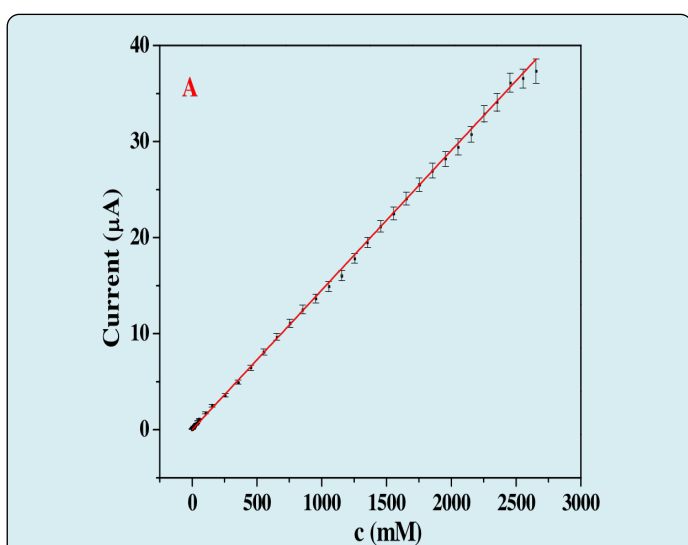


Figure 3: The corresponding calibration curve of the $\text{MnO}_2/\text{GNRs}/\text{GCE}$ in the H_2O_2 concentration range of 0.25–2455 M. limit of 0.071 M ($S/N = 3$) could be obtained. The proposed sensor displayed excellent electrochemical analytical performance, acceptable reproducibility, high accuracy, and great anti-interference ability [74].

Series of FeVO_4 materials with different morphologies were prepared in Yu Y [76] through a facile hydrothermal method and were studied as peroxidase mimics. The different pH values during the preparation process led to different crystal structures, morphologies, and peroxidase-like activities of the as-prepared FeVO_4 products. FeVO_4 nanobelts exhibited good selectivity, reproducibility, long-term stability, and easy recovery property benefited from its chemical stability and magnetic property. This work provides a novel, fast response, low cost, accessible, and highly sensitive system for visual detection of H_2O_2 .

Nanozyme, as the next-generation artificial enzyme, has attracted wide interest in recent years [57]. Compared

with natural enzymes, nanozyme, with their advantages of high stability against denaturing, low-cost, easy storage, and treatment is attractive and promising candidate in chemical sensing, immunoassay development, cancer diagnostics and therapy, and environmental protection [58]. At present, a large number of nanoparticle (NP) artificial enzymes have been constructed to mimic natural enzymes, including iron oxide-based NPs with peroxidase and catalase-like activities [59,60], cerium oxide-based nanomaterials with oxidase, catalase and SOD mimetic properties [61,62], cobalt oxide ones that are peroxide and catalase mimics [63,64], copper oxide and manganese dioxide nanomaterials that display oxidase-like activity [65, 66], vanadium pentoxide peroxidase mimics [67], and metal/bimetal-based [68] and carbon-based NPs [69] with oxidase, peroxidase, and SOD mimetic activity.

A new V_2O_5 nanozyme-based colorimetric assay has been developed for H_2O_2 and glucose detection. Under the optimal reaction conditions, the method showed good responses toward H_2O_2 with a linear range from 1 to 500 mM. The result shows that the proposed assay method for H_2O_2 and glucose based on V_2O_5 nanozyme has a wide linear range, and is simple, fast, and sensitive. It is reported about montmorillonite-loaded ceria nanocomposites with superior peroxidase-like activity for rapid colorimetric detection of H_2O_2 in [69].

Optical and Fluorescent Probes for Hydrogen Peroxide Detection

Rapid and sensitive detection of hydrogen peroxide in milk by an enzyme-free electrochemiluminescence sensor based on a polypyrrole-cerium oxide nanocomposite was proposed in Karimia A, et al. [77]. Highly sensitive electrochemiluminescence detection of mucin1 based on V_2O_5 nanospheres as peroxidase mimetics to catalyze H_2O_2 for signal amplification realized in Yang F, et al. [78]. An efficient Horseradish peroxidase chemiluminescence biosensor with surface imprinting based on phenylboronic acid-functionalized ionic liquid@magnetic graphene oxide was manufactured in Duan H, et al. [79]. Europium-doped GdVO_4 nanocrystals as a luminescent probe for hydrogen peroxide and for enzymatic sensing of glucose were investigated in Muhr V, et al. [80]. Rational designed benzochalcone-based fluorescent probe for molecular imaging of hydrogen peroxide in live cells and tissues was realized in Huang J, et al. [81]. A cyclic signal amplification strategy to fluorescence and the colorimetric dual-readout assay for the detection of H_2O_2 -related analytes and application to the colorimetric logic gate was developed in Chen H [82]. IR-780 dye-loaded chemiluminescent organic nanoparticles with near-infrared emission for hydrogen peroxide detection, and imaging were investigated in Wang T [83]. Optical Waveguides and

Integrated Optical Devices for Medical Diagnosis, Health Monitoring and Light Therapies were proposed. Different probes were proposed in Zhou Y, et al. [84-87].

Sensors Made of Porous Hydrogen Peroxide

Hydrogen peroxide sensors based on porous silicon are reported in Garreffo BP, et al. [88-92]. Electrosynthesis of gold nanoparticles/porous GaN electrode for non-enzymatic hydrogen peroxide detection was carried out in Miao-Rong Z [93]. Hydrogen peroxide sensors made from other porous composites are reported in Gong C, et al. [94-96]. Palladium nanoparticles supported on mesoporous silica microspheres for enzyme-free amperometric detection of H_2O_2 were released from living cells [97].

Sensors Made from Carbon Dots, Fibers, and Spheres

One-Step Hydrothermal Synthesis of N, Fe-Codoped Carbon Dots as Mimic Peroxidase and their Application on Hydrogen Peroxide and Glucose Detection was carried out in Li Y, et al. [98]. Let us mention also that one pot synthesis of nitrogen-doped hollow carbon spheres with improved electrocatalytic properties for sensitive H_2O_2 sensing in human serum was carried out in Peng C, et al. [99]. Enhanced selectivity and stability of ruthenium purple-modified carbon-fiber microelectrodes for detection of hydrogen peroxide in brain tissue was reported in Ledo A [100].

Single- and Multiwalled Carbon Nanotubes in the Detection of Hydrogen Peroxide

Room temperature monitoring of hydrogen peroxide vapor using platinum nanoparticles-decorated single-walled carbon nanotube networks was carried out in Dong-Jin Lee [101]. Hydrodynamic chronoamperometric determination of hydrogen peroxide was carried out using carbon paste electrodes coated by multiwalled carbon nanotubes decorated with MnO₂ or Pt particles [102].

H_2O_2 sensing enhancement by mutual integration of single-walled carbon nanohorns with metal oxide catalysts was shown in Bracamonte MV, et al. [103]. Electrocatalytic reduction of hydrogen peroxide by silver particles patterned on single-walled carbon nanotubes was discussed in Minh-Phuong Ngoc Bui [104].

Hydrogen Peroxide Sensors Made from Carbon Nanotubes

Our investigations of gas sensors made from different metal oxide composites with carbon nanotubes (CNTs) [105-

112] shown the following:

1. Use of pristine CNT as sensors does not promising.
2. Functionalization of CNTs can be made with organic materials. Hyper sensibility and selectivity of detection of CO_2 , NH_3 , O_2 , Cl_2 , HCl, dimetyldimetylphosphate observed by CNT nanocomposites, covered with polyethylene, polyaniline, and polypyrrol.
3. CNTs, decorated with Pd, Rh, Au and Ni nanoparticles are suggested for detection of H_2S , CH_4 , H_2 , CO, O_3 , C_6H_6 , NH_3 , NO_2 , and C_2H_5OH up to their ppb level.
4. Special interest is attended to the investigation of possibilities of manufacture of CNT functionalized (decorated) with different metal oxide composites. Most of its are carried out by CNT, decorated with SnO_2 . Modifications of such nanosensors surface with precious metals led to remarkable improve of the sensitivity and selectivity of sensors.
5. Sensibilisation of CNT- SnO_2 composites in water solutions of Ru (OH) Cl_3 leads to high response to hydrogen as well as to synergistic effect during detection of isobutene and the lowering of the temperature of pre-heating of work body of sensors up to 150-200°C. Such sensors are sensitive also to vapors of VOC gases (acetone, toluene, ethanol and methanol) at approving the same temperatures of pre-heating.
6. Thin film (including 1D film) nanosensors of ethanol vapors were manufactured on the base of CNT- Fe_2O_3 solid solutions. Sensors of H_2 , NO_x and CO were manufactured from CNTs with cobalt oxide, $Co_{1-x}N_xFe_2O_4$, CuO and WO_3 .
7. Substantial interest invokes research and development of nanosensors working without pre-heating of their work body (at room temperature). 10%- SnO_2 -CNT nanocomposites sensor detected ammonia and NO_2 . Doping of CNT with N and B and its synthesis with metal oxide SnO_2 allowed dramatically increase the conductivity of the nanosensor and response to CO and NO_2 . Nanosensors made from Co_3O_4 - SnO_2 and Pt/ TiO_2 /CNT were sensitive to H_2 , NH_3 and O_3 on the 20 ppb level of gas concentration.
8. Nanosensors made from all mentioned composites CNT-metal oxides had the lowest response and shorter times.
9. It is clear that the doping of metal oxides with CNTs leads to greater sensitivity to gases, better speed to response of nanosensors and a lowering of temperature of pre-heating of their work body (up to room temperature, when the pre-heating is not necessary). Possible mechanisms of the response of developed sensors to gases are discussed. Doubtless, that different types of conductivity of CNTs and metaloxides, change in the work function (high of potential barrier), modulation of formed heterojunctions should be take into account at the analysis of complicated processes and phenomena in gas sensitive structures reported above.

Solid-state VPHP sensors made from doped metal oxide $\text{ZnO}<\text{La}>$ and $\text{SnO}_2<\text{Co}>$ were prepared in Aroutiounian VM [113] for detection of H_2O_2 vapors. Ceramic targets made from metal oxide ZnO doped with 1 at.% La or SnO_2 doped with 2 at.% Co were synthesized by the method of solid-phase reaction in the air. The following program of annealing for the compact samples of $\text{ZnO}<\text{La}>$ was chosen: the rise of temperature from room temperature up to 1300 °C for three hours, soaking at this temperature for four hours, further decrease in the temperature for three hours prior to room temperature. The annealing of the compacted samples $\text{SnO}_2<\text{Co}>$ was carried out at 500°C, 700°C, 1000°C and 1100°C consecutively, soaking at each temperature for five hours. Then, the synthesized compositions were subjected to mechanical treatment in the air in order to eliminate surface defects. Thus, smooth, parallel targets with a diameter ~ 40 mm and thickness ~2 mm were manufactured. The prepared $\text{ZnO}<\text{La}>$ and $\text{SnO}_2<\text{Co}>$ targets had sufficient conductance and were used for the deposition of nanosize films. Multi-Sensor-Platforms (purchased from TESLA BLATNÁ, Czech Republic) are used as substrates. The platform integrates a temperature sensor (Pt 1000), a heater and interdigitated electrode structures with a platinum thin film on a ceramic substrate. The heater and the temperature sensor are covered with an insulating glass layer.

Gas sensitive layer made from ZnO doped with 1 at.% La or SnO_2 doped with 2 at.% Co was deposited onto the non-passivated electrode structures using the high-frequency magnetron sputtering method.

The measurements of the manufactured sensors' response (the sensor resistance changes under the influence of H_2O_2 vapors) were carried out at different concentrations of H_2O_2 vapors. The sensor work body temperature was varied from room temperature up to 350 °C. All measurements were carried out at the sensor applied voltage of 0.5 V. The thicknesses of the ZnO doped with 1 at.% La and SnO_2 doped with 2 at.% Co films were equal to 30 nm and 160 nm, respectively. The average size of nanoparticles was equal to 18.7 nm for both compositions. The sensors manufactured by us are resistive. The operation of this type of sensors grounds on the changes in the electrical resistance of gas-sensitive semiconductor layer under the influence of H_2O_2 vapors due to an exchange of charges between molecules of the semiconductor film and adsorbed H_2O_2 vapors.

The gas sensing properties of the prepared resistive type gas sensors made from doped metal oxide films under the influence of VPHP were investigated using a computer-controlled static gas sensor home-made test system (see [112]). The sensor was placed into a hermetic chamber. A certain quantity of the H_2O_2 water solution (10

mg) was injected in the measurement chamber. Different concentrations of HPV (from 100 ppm up to 4000 ppm) were reached in the chamber depending on the percentage content of the H_2O_2 water solution.

The measurements of the manufactured sensors' electrical resistance under the VPHP influence were carried out at different operating temperatures. The platinum heater located around the active surface of the sensor on Multi-Sensor-Platform ensures a necessary temperature of the working body. The sensor on the alumina substrate is placed on the heater which allows to rising temperature of the sensor's working body. All measurements of the electrical resistance were carried out at 0.5 V DC voltage applied on the sensor's electrode.

The typical response-recovery curves obtained as a result of these measurements for sensors with $\text{Zn}_{0.9929}\text{La}_{0.0071}\text{O}$ sensitive layer are presented in Figure 4. These films were deposited on alumina substrate during 15 minutes (Figure 4a) and 30 minutes (Figure 4b) and their thicknesses were equal to 80 nm and 210 nm, respectively. These characteristics demonstrate the change in the sensor's electrical resistance under the influence of 1800 ppm VPHP at different operating temperature. As a result of the measurements of sensing characteristics, the sensor response was calculated as the ratio $R_{\text{HPV}}/R_{\text{air}}$, where R_{HPV} is the sensor electrical resistance in the VPHP atmosphere and R_{air} is the sensor resistance in the air without VPHP. The results of such calculations of response for the $\text{SnO}_2<\text{Co}>$ sensor are presented in Figure 5. These measurements were carried out under the influence of 100 ppm VPHP at different working body temperatures measured at different operating temperatures for the $\text{Zn}_{0.9929}\text{La}_{0.0071}\text{O}$ sensors with films thicknesses of 80 nm (a) and 210 nm (b) [112]. Dependence of the sensor response on operating temperature (in insert) [112].

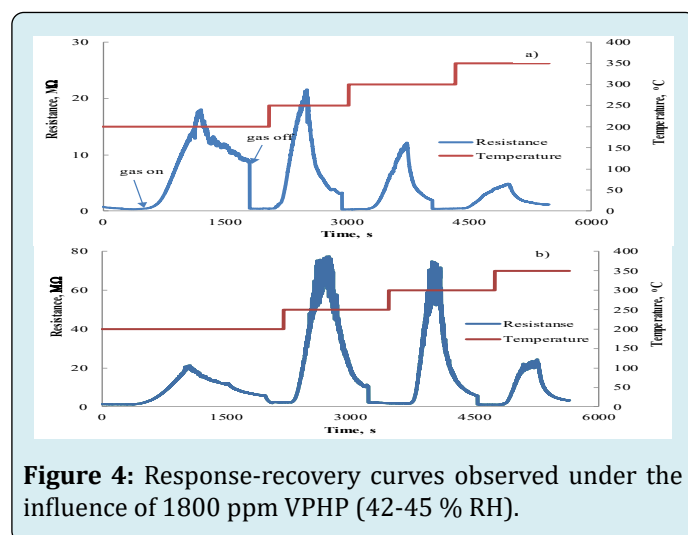


Figure 4: Response-recovery curves observed under the influence of 1800 ppm VPHP (42-45 % RH).

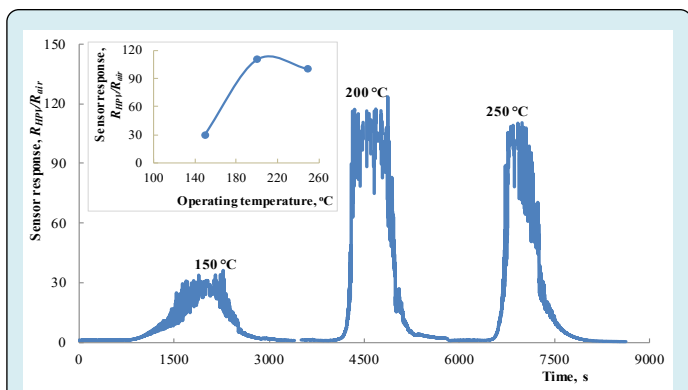


Figure 5: Response-recovery curves observed under the influence of 100 ppm HPV (42-45 % RH) measured at different operating temperatures for the $\text{SnO}_2\langle\text{Co}\rangle$ sensor.

The results of investigations of the dependence of the sensor response on operating temperature for sensors with the La-doped ZnO gas-sensitive layer are presented in Figure 6. The concentration μ of target gas was 1800 ppm in these measurements. At a relatively low operating temperature (150 °C), the best response was observed for the structure with a larger contents of impurity

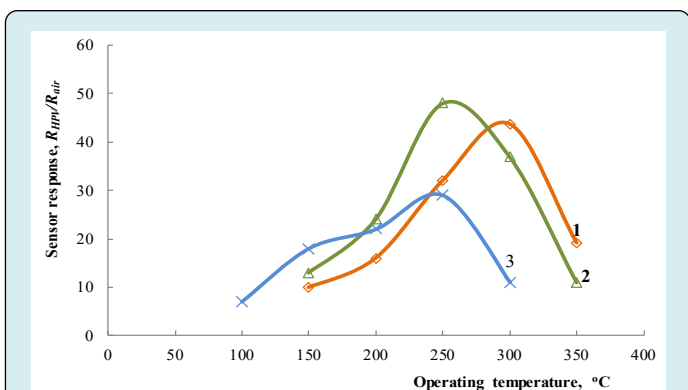


Figure 6: Dependence of the response to 1800 ppm of VPHP on operating temperature for the $\text{Zn}_{0.9929}\text{La}_{0.0071}\text{O}$ sensors on alumina substrate with films thicknesses of 80 nm (1) and 210 nm (2) and for the sensor with $\text{Zn}_{0.9853}\text{La}_{0.0147}\text{O}$ films deposited on Multi-Sensor-Platform (3) [112].

($\text{Zn}_{0.9853}\text{La}_{0.0147}\text{O}$). At higher temperatures, sensor with more thick film shows larger response. Probably a longer sputtering time allows obtaining a thicker film with a more perfect structure. Besides the roughness of the films' surfaces is the same since these sensitive layers were made under identical conditions. However, the working volume and, accordingly, the number of H_2O_2 molecules participating in the charge exchange process are larger for a thicker film.

Note, the electrical resistance of the prepared $\text{ZnO}\langle\text{La}\rangle$ sensors has changed in order of magnitude under influence

of VPHP starting at the operating temperature of 100 °C. However, a longer time is needed for the recovery of the sensors parameters at such temperature. The pulsed rise in the working body temperature needed for decreasing of the recovery time of the investigated sensors. The response and recovery times were determined when the time required for reaching the 90 % resistance changes from the corresponding steady-state value of each signal. For $\text{SnO}_2\langle\text{Co}\rangle$ structure both the response and recovery times were equal to 5 minutes at temperatures more than 200 °C. For the $\text{ZnO}\langle\text{La}\rangle$ sensors the response and recovery times were an average equal to 6-8 minutes and 10-12 minutes, respectively, at the operating temperatures more than 200 °C. The real response times may be less than the mentioned values. This is due to the fact that, as was already noted, 10 mg of an aqueous solution with a certain percentage content of H_2O_2 is injected in the measuring chamber in order to obtain the appropriate concentration of VPHP. The response time of the sensor, calculated from the moment when the H_2O_2 water solution is injected in the chamber until the maximum response reaches 90% .

As shown in Figure 5 and Figure 6, the sensor response decreases for both structures, when the temperature of the working body exceeds some certain value (250-300 °C and 200 °C for La-doped ZnO and Co-doped SnO_2 sensors, respectively). The number of vapor molecules adsorbed on a surface and generally kept by Van der Waals forces (physical adsorption), decreases with the increasing of temperature. More intensive exchange of electrons between the adsorbent and the adsorbed molecules takes place when the stronger chemical nature bond is established between them, originated at capping of electronic shells of both adsorbent and adsorbate atoms. The amount of chemisorbed centers increases with increasing in temperature. Desorption prevails over the adsorption when a temperature is increased above a certain value and, therefore, the sensor response decreases. The temperature of the sensors made of $\text{ZnO}\langle\text{La}\rangle$ structure, above which the sensitivity decreasing occurs, is greater than for the sensors made of $\text{SnO}_2\langle\text{Co}\rangle$ structure. Probably, the chemical bonds between molecules of ZnO and H_2O_2 are stronger than those between molecules of SnO_2 and H_2O_2 . The fact that the recovery time for sensors made of Co-doped SnO_2 is less than that for La-doped ZnO sensors also testifies the above-mentioned which the sensitivity decreasing occurs, is greater than for the sensors made of $\text{SnO}_2\langle\text{Co}\rangle$ structure. Probably, the chemical SnO_2 and H_2O_2 . The fact that the recovery time for sensors made of The permissible limit of exposure of 1,0 ppm is immediately dangerous for life and health when its concentration reaches 75 ppm. Therefore, it was necessary to investigate the gas sensing characteristics of prepared sensors made from doped metal oxide films at low concentrations of VPHP.

Such measurements of the sensing properties of the prepared sensors with La-doped ZnO and Co-doped SnO₂ sensitive films deposited on Multi-Sensor-Platforms were carried out at less than 100 ppm concentrations of VPHP. The results of these investigations are presented in Figure 7 and Figure 8. The measurements of the sensing characteristics of the sensors with Zn_{0.9929}La_{0.0071}O sensitive layer to 10 ppm VPHP were carried out in the following way. Firstly, an atmosphere containing 10 ppm of VPHP was prepared in a laboratory model of an isolator. This VPHP concentration decreased by spontaneous decomposition of H₂O₂. When a reference device (Dräger Sensor® H₂O₂ HC) could not detect any VPHP, the ZnO<La> sensor was inserted into the model isolator. Then, the sensor responded immediately. When the maximum response was reached, the sensor was taken out into an atmosphere without any traces of VPHP. This process was repeated three times (Figure 7a). In these studies, a voltage on the sensor at direct current is used as a parameter for sensing characteristics. The measurements of the sensing characteristics under the influence of 75 ppm VPHP were carried out using the same way for the SnO₂<Co> sensors (Figure 7b).

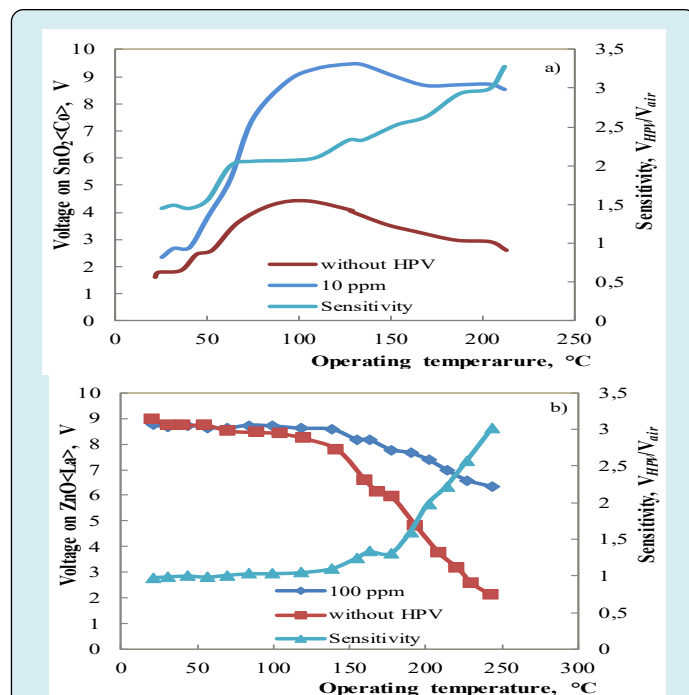
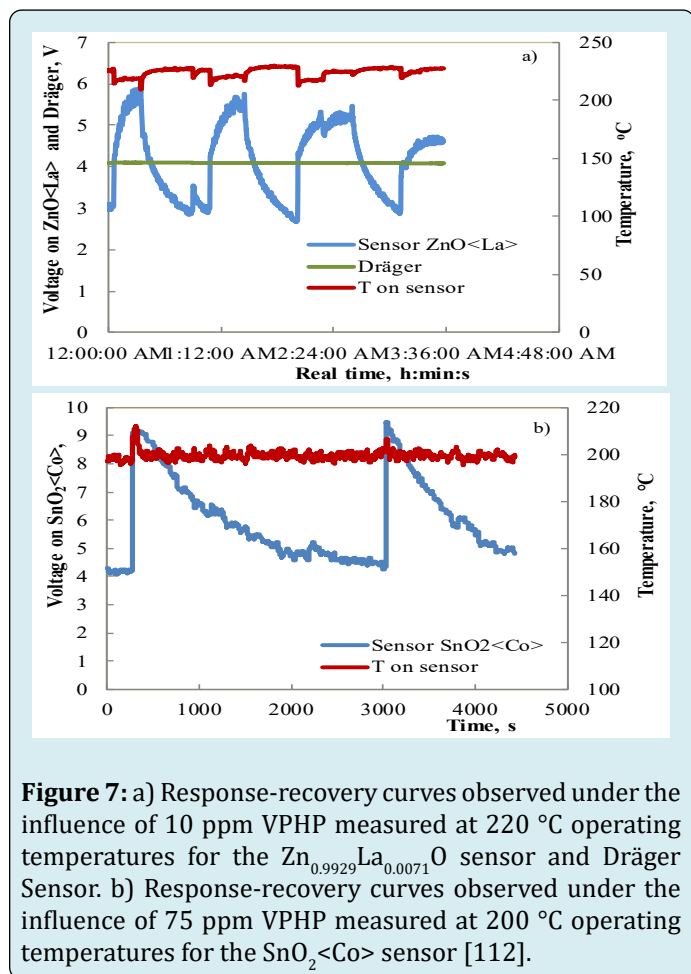


Figure 8: a) The temperature dependencies of voltage on sensor and sensitivity (V_{HPV}/V_{air}) for SnO₂<Co> sensor measured under the influence of 10 ppm VPHP (20-23 % RH) at 200 °C operating temperature. b) The temperature dependencies of voltage on sensor and sensitivity (V_{HPV}/V_{air}) for Zn_{0.9929}La_{0.0071}O sensor measured under the influence of 100 ppm VPHP at 220 °C operating temperature [112].

The temperature dependence of sensing parameter (or voltage on the sensor) under the influence of 10 ppm VPHP has investigated for the SnO₂<Co> sensors. For these measurements, the atmosphere in the “Peroxybox” system developed in the same Institute in Prague was controlled (0-10 ppm VPHP and 20-23 % RH) and the sensor’s temperature was changed. The final sensitivity was calculated as the voltage on the sensor in “Peroxybox” system VPHP divided by voltage on sensor in the air V_{air} (Figure 8a). The temperature dependence of sensing parameter under the influence of 100 ppm VPHP was investigated using the same way for the ZnO<La> sensors (Figure 8b).

The investigations of the prepared sensors under the influence of low concentrations of VPHP showed that the sensitivity (V_{HPV}/V_{air}) to 10 ppm of H VPHP was equal to ~ 2 for the ZnO<La> sensors at the working body temperature of 220 °C. Note that the DrägerSensor® H₂O₂ HC reference device was not sensitive to 10 ppm of VPHP (Figure 7a). The investigations of the sensors sensitivity’ to very low concentrations (0-10 ppm) of VPHP showed that the structure made of SnO₂<Co> exhibits a response to 10 ppm of VPHP at the operating temperature starting from 50 °C

(Figure 8a). The sensitivity to 10 ppm of VPHP was equal to ~ 3 for the $\text{SnO}_2<\text{Co}>$ sensors at the working body temperature of 200°C (Figure 9).

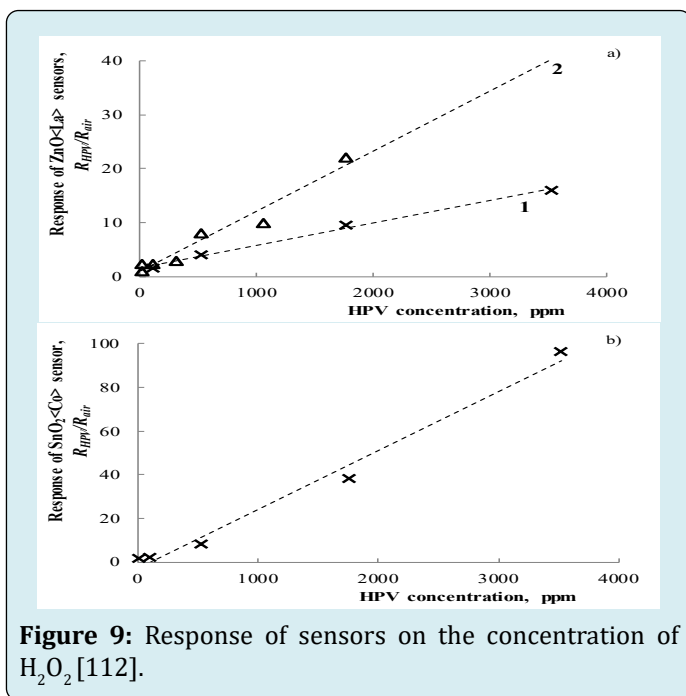


Figure 9: Response of sensors on the concentration of H_2O_2 [112].

So, it was found that both Co-doped SnO_2 and La-doped ZnO sensors exhibit a good response to VPHP starting at 100°C operating temperature. Sensors made from $\text{SnO}_2<\text{Co}>$ and $\text{ZnO}<\text{La}>$ were sufficiently sensitive to 10 ppm of VPHP. It was established that the dependencies of the response on VPHP concentration at the operating temperature of 150°C have a linear character for prepared structures and can be used for the determination of VPHP concentration.

Breath biomarkers for various diseases

The breath analysis is a promising method for rapid, inexpensive, non-invasive disease diagnosis and health monitoring owing to the correlative relationship between breath biomarker concentrations and abnormal health conditions. Breath biomarkers for various diseases are listed in Table 1 of the papers Aroutiounian VM [114,115].

Hydrogen peroxide is normally present in exhaled breath. Activation of airway epithelial and endothelial cells, neutrophils, alveolar macrophages, and eosinophils leads to the production of superoxide radicals and hence H_2O_2 production in airway inflammation. Note also that H_2O_2 with its neutral and low molecular weight allowing it to cross membranes to exit into the extracellular spaces. But it is less stable than other oxidative stress markers such as the isoprostanes. H_2O_2 is volatile thus its presence can be easily detected in exhaled beam condensate (EBC) as a marker of

pulmonary inflammation and oxidative stress.

Many studies analyzing exhaled breath condensate (EBC) of H_2O_2 have used spectrophotometric assays [116-120], fluorimetric assay [121], injection analysis with fluorescence detection by chemiluminescent methods, and by immediate online analysis with a commercially available amperometric biosensor of Ecocheck, Jaeger, Germany. Although chemiluminescent methods have high sensitivity, detecting H_2O_2 in the nanomolar range, they are limited by poor day-to-day precision and typically require expensive equipment, which may not be present during routine clinical studies. Note that all mentioned methods are rather expensive and cannot use out of medical hospitals. To overcome the challenges associated with spectroscopic and/or MS techniques for breath analysis of respiratory diseases, semiconductor chemical sensors have been adopted [122].

We have to take into account that H_2O_2 has significant increase in exhaled breath, compared to healthy subjects, in patients with asthma, chronic obstructive pulmonary disease (COPD), bronchiectasis, acute respiratory distress syndrome, interstitial lung disease [114,115]. Breathing patterns must be taken into consideration with all EBC H_2O_2 measurements.

It was mentioned above that H_2O_2 is elevated in exhaled air condensate of ill peoples with stable asthma, and may reflect airway inflammation [123]. Exhaled air condensate has been proposed as a noninvasive means of obtaining samples from the lower respiratory tract, based on the hypothesis that aerosol particles excreted in breath may reflect the composition of the lower airway fluids [124]. Inflammatory cells produce H_2O_2 , which causes lung inflammation and damage [125,126]. Indeed, increased content of H_2O_2 has been described in various inflammatory lung disorders: in exhaled air of cigarette smokers [127]; patients with adult respiratory distress syndrome (ARDS) [128-130]; and patients with acute hypoxaemic respiratory failure [130].

The study in Jobsis Q [131] demonstrated a significantly increased concentration of H_2O_2 in exhaled air condensate from stable asthmatic children compared to healthy controls. Correlation of H_2O_2 in exhaled air condensate with invasive measures of airway inflammation, such as bronchial biopsies, is needed to validate the hypothesis that exhaled peroxide reflects airway inflammation. The concentration of H_2O_2 in exhaled air is a potentially useful marker of airway inflammation in asthmatics, especially since the procedure is quick and easy to perform. Further studies should explore its value as a noninvasive test, e.g. for monitoring the effects of anti-inflammatory therapy [131]. The study has shown that the concentration of H_2O_2 in exhaled air condensate is increased in stable asthmatic children, and lower in patients

receiving anti-inflammatory treatment, suggesting that airway inflammation increases exhaled peroxide. Correlation of H_2O_2 in exhaled air condensate with invasive measures of airway inflammation, such as bronchial biopsies, is needed to validate the hypothesis that exhaled peroxide reflects airway inflammation. The concentration of hydrogen peroxide in exhaled air is a potentially useful marker of airway inflammation in asthmatic children, especially since the procedure is quick and easy to perform.

Low-dose CT followed by bronchoscopy in lung cancer is still the main standard procedure in the diagnosis and monitoring process despite high numbers of false-positive cases. Sensor technology for breath analysis may solve this problem and reduce the number of false positives. As it was shown in Moller W, et al. [132], investigations of sensors in exhaled breath condensate (EBC) allow non-invasive monitoring of inflammation in the lung. Activation of inflammatory cells results in an increased production of reactive oxygen species, leading to the formation of H_2O_2 . Cigarette smoking induces an inflammatory response in the airways that may play a key role in the pathogenesis of COPD. Investigations carried out in Moller W, et al. [132] are shown that the concentration of H_2O_2 was 2.6 times higher in the airway versus the alveolar fraction. Airway H_2O_2 was twofold higher in smokers and fivefold higher in COPD patients compared to non-smokers.

Many lung diseases cause inflammation at different sites of the lung, therefore fractionated sampling of EBC can reduce variability and maintain an anatomical allocation of the exhaled biomarkers. Inflammatory processes in the lung elicit so-called oxidative stress, meaning that the integrity of the lung is jeopardized by oxidants, and the latter process is supposed to play an important role in the development of COPD [133,134]. Oxidative stress is known to be increased in both stable and unstable COPD patients, due to either exposure to exogenous oxidants as present in cigarette smoke, in air pollution or as enhanced endogenous production of H_2O_2 . Excessive production of oxidants may lead to oxidative damage to the tissue [135,136]. Sputum induction has been used for studying airway inflammation [137], but because of the risk of aggravating the exacerbation, induced sputum may not be appropriate during exacerbation.

Increased levels of exhaled hydrogen peroxide in EBC of smoker and COPD patients were reported previously [127,138,139]. The higher release of H_2O_2 in the airways compared to the alveolar space is not similarly evident. It may depend on the inhalation of environmental particles with preferred deposition in the airways. Because of the much smaller surface area of the airways compared to the alveolar space, the airways have an up to 10-fold higher density of deposited particles [140,141]. These

particles, although cleared by more efficient mechanisms [142,143], can stimulate defense cells to cause low-level oxidative stress and the release of H_2O_2 [144]. EBC provides a non-invasive means of sampling the lower respiratory tract [145-148].

Non-invasive measurements of characteristics of H_2O_2 sensors in EBC is useful to detect the oxidative destruction of the lung as well as early inflammation of the airways in a healthy individual with risk factors and comparing the inflammatory response to treatment [146,148]. This study helps to validate the analysis of EBC by measuring hydrogen peroxide (H_2O_2) concentration in healthy non-smokers, smokers, diseased, and also comparing the response to treatment. Inflammatory cells release H_2O_2 , which can be detected in EBC in a measuring chamber containing biosensors [132]. Elevated levels of H_2O_2 have been found in a number of respiratory disorders, thus H_2O_2 is considered to be a possible biomarker of airway inflammation. H_2O_2 was one of the most commonly studied markers in EBC [149,150]. The lung is constantly exposed to oxygen, so highly susceptible to oxidative stress in the form of reactive oxygen species (superoxide ion, hydroxyl radical, and hydrogen peroxide). These reactive oxygen species are produced by active inflammatory cells like neutrophils, macrophages, activated eosinophils, epithelial cells, and endothelial cells [152]. Exhaled H_2O_2 was 5×10^4 times lower than H_2O_2 produced in the alveolar lining fluid. This difference was attributed to the presence of antioxidants in the lining fluid of the lower respiratory tract. The level of H_2O_2 in exhaled breath condensate of smokers is increased half-hour after combustion of one cigarette. The levels of H_2O_2 were elevated in healthy smokers and also in healthy non-smokers who are residing an urban area compared to those of rural area. These elevated levels can be attributed to constant exposure to vehicle and industrial pollution. Levels of H_2O_2 also correlated with eosinophils differential counts in induced sputum. Bronchiectasis, a suppurative lung disease, is characterized by significant pulmonary oxidant stress that can be measured using exhaled breath H_2O_2 . Patients with bronchiectasis displayed exhaled H_2O_2 levels higher than normal controls. In the studied cases of bronchiectasis, H_2O_2 was raised significantly with a reduction in the levels following treatment. Patients with rheumatoid arthritis with interstitial lung diseases had increased levels of exhaled H_2O_2 , suggesting that EBC H_2O_2 is a potentially useful biomarker.

The measurement of the H_2O_2 marker EBC can be used routinely for i) early prediction of the ongoing inflammatory process in healthy individuals who are exposed to risk factors, ii) early tool of assessing exacerbation of the lung condition and to reduce the morbidity, iii) as a marker in assessing the inflammatory response to treatment. Hence, the detection of H_2O_2 in EBC can be used for routine clinical practice and

research activities.

As was mentioned above, the analysis of H_2O_2 in EBC has several advantages over other methods for assessing lung inflammation [152]. The identification of selective profiles of inflammatory markers in EBC might also be of diagnostic value in patients with COPD. Such analysis is completely non-invasive. Analysis of EBC has shown an influence of apocynin inhalation on H_2O_2 production in comparison to placebo inhalation [151]. H_2O_2 concentration after 60 minutes of apocynin inhalation was significantly lower. Apocynin caused a significant decline of H_2O_2 concentration, not causing any side effects. Therefore, the inhibitory of this drug act as a strong anti-inflammatory agent.

Another method of determining the degree of oxidative stress is the collection of exhaled breath condensate (EBC) and the analysis of H_2O_2 [153-155]. H_2O_2 biological markers have been identified in EBC, which play a role in inflammatory processes [155-158]. EBC- H_2O_2 was higher during exacerbation than during stable disease in COPD patients and inhaled antioxidants and corticosteroids can reduce the level of exhaled H_2O_2 [159,160]. In addition, EBC-pH has provided data supporting the important role of acidic stress in respiratory diseases [161]. EBC- H_2O_2 was higher during exacerbation than during stable disease in COPD patients and inhaled antioxidants and corticosteroids can reduce the level of exhaled H_2O_2 [162- 166]. In addition, EBC-pH has provided data supporting the important role of acidic stress in respiratory diseases [167].

The concentration of the biomarkers and H_2O_2 in exhaled breath condensate in healthy and disease shows great variation among subjects and among laboratories [168]. Respiratory symptoms were obtained using a questionnaire [163] and pulmonary function parameters were measured by spirometry and body plethysmography (Jäger Masterlab, Erich Jaeger GmbH, Höchberg, Germany) [164]. Exhaled breath condensate was collected using the ECoScreen-2 (Filt GmbH, Berlin, Germany). Because the ECoScreen-2 device does not store the flow profile of each breath and because we wanted to visualize the breathing on a PC monitor, an additional spirometer device (Spiro Pro, Erich Jaeger GmbH, Höchberg, Germany) was coupled between ECoScreen-2 and the subjects mouth piece. Flow and volume were recorded continuously and analyzed for tidal volume and exhalation flow rates.

Chemical sensors for breath analysis of cancer based on chemiresistors using gold nanoparticles (GNPs) and/or SWCNTs are the most examined sensing technologies for cancer-based detection by breath sampling. Using these sensor arrays, Peng, et al. [132] and Nakhleh, et al. [134] showed their use in detecting and classifying many types of

cancer, opening a window for developing a multi-applicable sensor technology for clinical practice. Sensors for breath detecting pulmonary arterial hypertension; obstructive sleep apnoea syndrome; cystic fibrosis, and tuberculosis from exhaled breath are also reported in the paper [134]. Carbon black polymer composite, MO-metal oxide, single-walled carbon nanotubes, silicon nanowire field effect transistors, monolayer-capped metal-coated nanoparticles as well as quartz microbalance devices were used. Note also that graphene dispersed cellulose microfibers composite are proposed for efficient immobilization of hemoglobin and selective biosensor for detection of hydrogen peroxide [168].

Very promising and modern electronic-nose technics are used during measurements of breath, the early detection of early lung cancer, screening of obstructive sleep apnea syndrome, early diagnosis of gastrointestinal diseases, breath tests for pneumoconiosis of active tuberculosis chronic pulmonary infections, inflammatory asthma, COPD in respiratory medicine [169-190]. It was shown and discussed in Aroutiounian VM [191-193], we can wait for that after choosing the most sensitive sensors to hydrogen peroxide at its low concentrations, which occur when the patient exhales air, and determining their low cost, a microelectronic device with an Arduino New microprocessor will be implemented for accurate digital determination of the degree of the above disease, which will be tested by doctors and recommended for use.

Conclusion

The results of studies of many types of semiconductor H_2O_2 sensors are discussed in this review of 175 articles about hydrogen peroxide. The properties of electrochemical detectors, sensors based on organic and inorganic materials, graphene, and nano-sensors are analyzed. Optical and fluorescent sensors, detectors made of porous materials, quantum dots, fibers, and spheres are briefly discussed. The results of our studies in the YSU of hydrogen peroxide sensors made from solid solutions of carbon nanotubes with semiconducting metal oxides are also presented in the review. The fundamentals of the manufacture of biomarkers of respiration containing hydrogen peroxide vapors, which make it possible to judge the degree of a person's illness with various respiratory diseases (asthma, tongue cancer, etc.), are discussed.

After choosing the most sensitive sensors to hydrogen peroxide at its low concentrations, which occurs when the patient exhales air, and determining their low cost, a microelectronic device with an Arduino microprocessor will be implemented for accurate digital determination of the degree of the above disease, which will be tested by doctors and recommended for use.

References

1. Ai F, Chen H, Zhang SH, Liu SY, Wei F, et al. (2009) Real-time monitoring of oxidative burst from single plant protoplasts using microelectrochemical sensors modified by platinum nanoparticles. *Anal Chem* 81(20): 8453-8458.
2. Hsu CC, Lo YR, Lin YC, Shi YC, Li PLA (2015) Spectrometric Method for Hydrogen Peroxide Concentration Measurement with a Reusable and Cost-Efficient Sensor. *Sensors* 15(10): 25716-25729.
3. Rahim HA, Morat BC, Rahim RA (2011) Non-Invasive Evaluation of Hydrogen Peroxide Concentrations in a Drinking Bottle by Near-Infrared Spectrometry. *Sensors & Transducers* 131(8): 83-90.
4. Sun J, Li C, Qi Y, Guo S, Liang X (2016) Optimizing Colorimetric Assay Based on V2O5 Nanozymes for Sensitive Detection of H₂O₂ and Glucose. *Sensors* 16(4): 584.
5. Chen W, Cai S, Ren QQ, Wen W, Zhao YD (2012) Recent advances in electrochemical sensing for hydrogen peroxide: a review. *Analyst* 117(1): 137.
6. Chen S, Yuan R, Chai Y, Hu F (2013) Electrochemical sensing of hydrogen peroxide using metal nanoparticles: a review. *Microchimica Acta* 180: 15-32.
7. Chen X, Wu G, Cai Z, Oyama M, Chen X, et al. (2014) Advances in enzyme-free electrochemical sensors for hydrogen peroxide, glucose, and uric acid. *Microchimica Acta* 181: 689-705.
8. Puganova EA, Karyakin AA (2005) New materials based on nanostructured Prussian blue for development of hydrogen peroxide sensors. *Sensors and Actuators B Chemical* 109(1): 167-170.
9. Kacer P, Svrcek J, Syslová K, Václavík J, Pavlík D, et al. (2012) Vapor Phase Hydrogen Peroxide – Method for Decontamination of Surfaces and Working Areas from Organic Pollutants. *InTech*, pp: 430.
10. Taizo I, Sinichi A, Kawamura K (1998) Application of a newly developed hydrogen peroxide vapor phase sensor to HPV sterilizer. *PDA J Pharm Sci Technology* 52(1): 13-18.
11. Mills A, Grosshans P, Snadden E (2009) Hydrogen peroxide vapour indicator. *Sens & Actuators B-Chemical* 136(2): 458-463.
12. Corveleyn S, Vandenbossche GMR, Remon JP (1997) Near-infrared (NIR) monitoring of H₂O₂ vapor concentration during vapor hydrogen peroxide (VHP) sterilization. *Pharm Res* 14(3): 294-298.
13. Novák M Bach (2013) Thesis. University of Chemistry and Technology, Prague.
14. Bohrer FI, Colesniuc CN, Park J, Schuller IK, Kummel AC, et al. (2008) Selective Detection of Vapor Phase Hydrogen Peroxide with Phthalocyanine Chemiresistors. *J Amer Chem Soc* 130(12): 3712-3713.
15. Zhang T, Yuan R, Chai Y, Li W, Ling S (2008) A Novel Nonenzymatic Hydrogen Peroxide Sensor Based on a Polypyrrole Nanowire-Copper Nanocomposite Modified Gold Electrode. *Sensors* 8(8): 5141-5152.
16. Benedet J, Lu D, Cizek K, Belle JL, Wang J (2018) Amperometric sensing of hydrogen peroxide vapor for security screening. *Anal Bioanal Chem* 395(2): 371-376.
17. Naik AN, Patra S, Kanekara AS, Sen D, Ramagiri SV, et al. (2018) Nafion membrane incorporated with silver nanoparticles as optical test strip for dissolved hydrogen peroxide: Preparation, deployment and the mechanism of action. *Sensors Actuators B: Chemical* 255: 605-615.
18. Yanzi Wu, Yujie Ma, Xu G, Wei F, Ma Y, et al. (2017) Metal-organic framework coated Fe₃O₄ magnetic nanoparticles with peroxidase-like activity for colorimetric sensing of cholesterol. *Sensors Actuators B: Chemical* 249: 195-202.
19. Kon Y, Usui Y, Sato K (2007) Oxidation of allylic alcohols to α,β -unsaturated carbonyl compounds with aqueous hydrogen peroxide under organic solvent-free conditions. *Angew Chem* 119: 5623.
20. Hea J, Sunarso J (2019) *J Hazardous Materials* 2: 118.
21. Chia-Wei H, Valinton JAA, Hung Y, Chen Ch (2018) Facet-specific heterojunction in gold-decorated pyramidal silicon for electrochemical hydrogen peroxide sensing. *Sensors and Actuators B: Chemical* 266: 463-471.
22. Yotam YA, Dotan H, Klotz D, Grave DA, Tsyganok A (2018) Two-site H₂O₂ photo-oxidation on haematite photoanodes. *Nature Communications* 9: 4060.
23. Ragavan KV, Ahmed RS, Weng X, Neethirajan S (2018) Chitosan as a peroxidase mimic: Paper based sensor for the detection of hydrogen peroxide. *Sensors and Actuators B: Chemical* 272: 8-13.
24. Busa LSA, Maeki M, Ishida M, Tani H, Tokeshi M (2016) Simple and sensitive colorimetric assay system for horseradish peroxidase using microfluidic paper-based devices. *Sensors and Actuators B: Chemical* 236: 433-

- 441.
25. Yagati AK, Lee T, Min J, Choi JW (2010) Amperometric sensor for hydrogen peroxide based on direct electron transfer of spinach ferredoxin on Au electrode. *Bioelectrochemistry* 80(2): 169-174.
 26. Zhang L, Chen M, Jiang Y, Chen M, Ding Y, et al. (2017) A facile preparation of montmorillonite-supported copper sulfide nanocomposites and their application in the detection of H₂O₂. *Sensors and Actuators B: Chemical* 239: 28-35.
 27. Jin D, Sakthivel K, Gandhi S, Huy BT, Lee Y (2016) An improved non-enzymatic hydrogen peroxide sensor based on europium functionalized inorganic hybrid material-Evaluation of optical and electrochemical properties. *Sensors and Actuators B: Chemical* 237: 81-89.
 28. Lorencova L, Bertok T, Filip J, Jerigova M, Velic D, et al. (2018) Highly stable Ti₃C₂T_x (MXene)/Pt nanoparticles-modified glassy carbon electrode for H₂O₂ and small molecules sensing applications. *Sensors and Actuators B: Chemical* 263: 360-368.
 29. Yu G, Wu W, Pan X, Zhao Q, Wei X, et al. (2015) High Sensitive and Selective Sensing of Hydrogen Peroxide Released from Pheochromocytoma Cells Based on Pt-Au Bimetallic Nanoparticles Electrodeposited on Reduced Graphene Sheets. *Sensors* 15(2): 2709-2722.
 30. Sahin OG (2015) *Electrochimica Acta* 180: 87.
 31. Zhang X, Bi X, Di W, Qin W (2016) A simple and sensitive Ce(OH)CO₃/H₂O₂/TMB reaction system for colorimetric determination of H₂O₂ and glucose. *Sensors and Actuators B: Chemical* 231: 714-722.
 32. Ding Y, Yang B, Liu H, Liu Z, Zhang X, et al. (2018) FePt-Au ternary metallic nanoparticles with the enhanced peroxidase-like activity for ultrafast colorimetric detection of H₂O₂. *Sensors and Actuators B: Chemical* 259: 775-783.
 33. Thiagarajan S, Buo-Wei S, Chen SM (2009) Nano TiO₂-Au-KI film sensor for the electrocatalytic oxidation of hydrogen peroxide. *Sensors and Actuators B: Chemical* 136(2): 464-471.
 34. Asifa M, Haitaoa W, Shuang D, Aziz A, Zhang G, et al. (2017) Metal oxide intercalated layered double hydroxide nanosphere: With enhanced electrocatalytic activity towards H₂O₂ for biological applications. *Sensors and Actuators B: Chemical* 239: 243-252.
 35. Cao GS, Wang P, Li X, Wang Y, Wang G, Li J (2015) A sensitive nonenzymatic hydrogen peroxide sensor based on Fe₃O₄-Fe₂O₃ nanocomposites. *Bull Mater Sci* 38: 163-167.
 36. Chaichi MJ, Ehsani M (2016) A novel glucose sensor based on immobilization of glucose oxidase on the chitosan-coated Fe₃O₄ nanoparticles and the luminol-H₂O₂-gold nanoparticle chemiluminescence detection system. *Sensors and Actuators B: Chemical* 223: 713-722.
 37. Liu H, Ding Y, Yang B, Liu Z, Liu Q, et al. (2018) Colorimetric and ultrasensitive detection of H₂O₂ based on Au/Co₃O₄-CeOx nanocomposites with enhanced peroxidase-like performance. *Sensors and Actuators B: Chemical* 271: 336-345.
 38. Aneesh K, Srinivasa Ch, Berchmans S (2017) Enhanced peroxidase-like activity of CuWO₄ nanoparticles for the detection of NADH and hydrogen peroxide. *Sensors and Actuators B: Chemical* 253: 723-730.
 39. Lua W, Suna Y, Dai H, Ni P, Jiang S, et al. (2016) Direct growth of pod-like Cu₂O nanowire arrays on copper foam: Highly sensitive and efficient nonenzymatic glucose and H₂O₂ biosensor. *Sensors and Actuators B: Chemical* 231: 860-866.
 40. Chakrabarti S, Panja R, Roy S, Roy A, Samanta S, et al. (2018) Evolution of resistive switching mechanism through H₂O₂ sensing by using TaOx-based material in W/Al₂O₃/TaOx/TiN structure. *Appl Surf Sci* 433: 51-59.
 41. Aroutiounian VM (2019) Non-Invasive Metal Oxide Sensors on Exhaled Aceton. *J Contemp Physics (Arm Acad Sci)* 54: 117-132.
 42. Lin CY, Chang CT (2015) Iron oxide nanorods array in electrochemical detection of H₂O₂. *Sensors and Actuators B: Chemical* 220: 695-704.
 43. Li X, Du X (2017) Molybdenum disulfide nanosheets supported Au-Pd bimetallic nanoparticles for non-enzymatic electrochemical sensing of hydrogen peroxide and glucose. *Sensors and Actuators B: Chemical* 239: 536-543.
 44. Hu J, Zhang C, Li X, Du X (2020) An Electrochemical Sensor Based on Chalcogenide Molybdenum Disulfide-Gold-Silver Nanocomposite for Detection of Hydrogen Peroxide Released by Cancer Cells. *Sensors* 20(23): 6817.
 45. Wang M, Jiang X, Liu J, Guo H, Liu C (2015) Highly sensitive H₂O₂ sensor based on Co₃O₄ hollow sphere prepared via a template-free method. *Electrochimica*

- Acta 182: 613-620.
46. Chen W, Cai S, Ren QQ, Wen W, Zhao YD (2012) Recent advances in electrochemical sensing for hydrogen peroxide: a review. *Analyst* 137: 49-58.
 47. Jia W, Guo M, Zheng Z, Yu T, Rodriguez EG, et al. (2009) Electrocatalytic oxidation and reduction of H₂O₂ on vertically aligned Co₃O₄ nanowalls electrode: Toward H₂O₂ detection. *J Electroanal Chem* 625: 27-32.
 48. Hou C, Xu Q, Yin L, Hu X (2012) (2012) Metal-organic framework templated synthesis of Co₃O₄ nanoparticles for direct glucose and H₂O₂ detection. *Analyst* 137(24): 5803.
 49. Ensafi AA, Jafari-Asl M, Rezaei B (2013) A novel enzyme-free amperometric sensor for hydrogen peroxide based on Nafion/exfoliated graphene oxide-Co₃O₄ **nanocomposite**. *Talanta* 103: 322-329.
 50. Heli H, Pishahang J (2014) Cobalt oxide nanoparticles anchored to multiwalled carbon nanotubes: Synthesis and application for enhanced electrocatalytic reaction and highly sensitive nonenzymatic detection of hydrogen peroxide *Electrochim Acta* 123(20): 518-526.
 51. Mu J, Zhang L, Zhao M, Wang Y (2013) Co₃O₄ nanoparticles as an efficient catalase mimic: Properties, mechanism and its electrocatalytic sensing application for hydrogen peroxide. *Journal of Molecular Catalysis A: Chemical* 378: 30-37.
 52. Xia S, Yu M, Hua J, Fenga J, Chen J, et al. (2014) A model of interface-related enhancement based on the contrast between Co₃O₄ sphere and cube for electrochemical detection of hydrogen peroxide. *Electrochem Commun* 40: 67-70.
 53. Shan G, Zheng S, Chen S, Chen Y, Liu Y (2013) Detection of label-free H₂O₂ based on sensitive Au nanorods as sensor. *Colloids and Surfaces B: Biointerfaces* 102: 327-330.
 54. Boca Raton, Aroutiounian Vladimir (2016) Graphene and graphene-oxide-based gas sensors. In: *Applications and Industrialization, Graphene Science Handbook*. CRC Press Taylor & Francis Group, USA, 20: 299.
 55. Wu X, Li F, Zhao C, Qian X (2018) One-step construction of hierarchical Ni(OH)₂/RGO/Cu₂O on Cu foil for ultra-sensitive non-enzymatic glucose and hydrogen peroxide detection. *Sensors and Actuators B: Chemical* 274: 163-171.
 56. Ebrahimi A, Zhang K, Dong C, Subramanian S, Butler D, et al. (2019) FeSx-graphene heterostructures: Nanofabrication-compatible catalysts for ultra-sensitive electrochemical detection of hydrogen peroxide. *Sensors and Actuators B: Chemical* 285: 631-638.
 57. Venegas CJ, Yedinaka E, Marco JF, Bollo S, Leon DR (2017) Co-doped stannates /reduced graphene composites: Effect of cobalt substitution on the electrochemical sensing of hydrogen peroxide. *Sensors and Actuators B: Chemical* 250: 412-419.
 58. Sharma V, Shaikh M (2017) Cytocompatible peroxidase mimic CuO:graphene nanosphere composite as colorimetric dual sensor for hydrogen peroxide and cholesterol with its logic gate implementation *Sensors and Actuators B: Chemical* 240: 338-348.
 59. Wang J, Sun HB, Pan HY, Ding YY, Wan JG, et al. (2016) Detection of hydrogen peroxide at a palladium nanoparticle-bilayer graphene hybrid-modified electrode. *Sensors and Actuators B: Chemical* 230: 690-696.
 60. Lorestani F, Shahnavaz Z, Mn P, Alias Y, Manan SAN (2015) One-step hydrothermal green synthesis of silver nanoparticle-carbon nanotube reduced-graphene oxide composite and its application as hydrogen peroxide sensor. *Sensors and Actuators B: Chemical* 208: 389-398.
 61. Wang H, Wang H, Li T, Ma J, Li K, et al. (2017) Silver nanoparticles selectively deposited on graphene-colloidal carbon sphere composites and their application for hydrogen peroxide sensing. *Sensors and Actuators B: Chemical* 239: 1205-1212.
 62. Jin GH, Ko E, Kim MK, Tran VK, Son SE, et al. (2018) Graphene oxide-gold nanozyme for highly sensitive electrochemical detection of hydrogen peroxide. *Sensors and Actuators B: Chemical* 274: 201-209.
 63. Kogularasu S, Govindasamy M, Chen SM, Akilarasan M, Mani V (2017) 3D graphene oxide-cobalt oxide polyhedrons for highly sensitive non-enzymatic electrochemical determination of hydrogen peroxide. *Sensors and Actuators B: Chemical* 253: 773-783.
 64. Chena X, Gaob J, Zhao G, Wu C (2020) In situ growth of FeOOH nanoparticles on physically-exfoliated graphene nanosheets as high performance H₂O₂ electrochemical sensor. *Sensors and Actuators B: Chemical* 313: 128038.
 65. Martinez A, Ibarra A, Estrada-Moreno IA, Osuna V, Dominguez RB (2019) Flexible electrochemical sensor based on laser scribed Graphene/Ag nanoparticles for non-enzymatic hydrogen peroxide detection. *Sensors and Actuators B: Chemical* 301: 127101.

66. Lu X, Liu X, Shen T, Qin Y, Zhang Pu, et al. (2017) Convenient fabrication of graphene/gold nanoparticle aerogel as direct electrode for H₂O₂ sensing. *Materials Letters* 207: 49-52.
67. Ni PM, Woi MP, Alias Y (2017) Facile one-step electrochemical deposition of copper nanoparticles and reduced graphene oxide as nonenzymatic hydrogen peroxide sensor. *Applied Surface Science* 413: 56-65.
68. Aroutiounian VM (2020) Acetone Sensor Made of Tin Dioxide. *J Contemp Phys (Arm Acad Sci)* 55: 213-224.
69. Sun L, Ding Y, Jiang Y, Liu Q (2017) Montmorillonite-loaded ceria nanocomposites with superior peroxidase-like activity for rapid colorimetric detection of H₂O₂. *Sens Actuators B: Chemical* 239: 848-856.
70. Li L, Du Z, Liu S, Hao Z, Wang Y, et al. (2010) A novel nonenzymatic hydrogen peroxide sensor based on MnO₂/graphene oxide nanocomposite. *Talanta* 82(5): 1637-1641.
71. Yu Z, Lin H, Zhang X, Liu N, Zhang X (2015) NiO/graphene nanocomposite for determination of H₂O₂ with a low detection limit. *Talanta* 144: 1-5.
72. Palanisamy S, Chen S, Sarawathi R (2012) A novel nonenzymatic hydrogen peroxide sensor based on reduced graphene oxide/ZnO composite modified electrode. *Sensors and Actuators B: Chemical* 166-167: 372-377.
73. Pogacean F, Socaci C, Pruneanu S, Biris AR, Coros M, et al. (2015) Graphene based nanomaterials as chemical sensors for hydrogen peroxide – A comparison study of their intrinsic peroxidase catalytic behaviour. *Sensors and Actuators B: Chemical* 213: 474-483.
74. Wu ZL, Li CK, Yu JG, Chen XQ (2017) MnO₂/reduced graphene oxide nanoribbons: Facile hydrothermal preparation and their application in amperometric detection of hydrogen peroxide. *Sensors and Actuators B: Chemical* 239: 544-532.
75. Huang S, Si Z (2016) *Ibid* 264: 155.
76. Yu Y, Ju P, Zhang D, Han X, Yin X, et al. (2016) Peroxidase-like activity of FeVO₄ nanobelts and its analytical application for optical detection of hydrogen peroxide. *Sensors and Actuators B: Chemical* 233: 162-172.
77. Karimia A, Husain SW (2018) *Ibid* 271: 290.
78. Yang F, Jiang X, Zhong X, Wei S, Yuan R (2018) Highly sensitive electrochemiluminescence detection of mucin1 based on V2O5 nanospheres as peroxidase mimetics to catalyze H₂O₂ for signal amplification. *Sensors and Actuators B: Chemical* 265: 126-133.
79. Duan H, Wang X (2016) *Ibid* 236: 244.
80. Muhr V, Buchner M, Hirsch T, Jovanović DJ, Dolić SD, et al. (2017) Europium-doped GdVO₄ nanocrystals as a luminescent probe for hydrogen peroxide and for enzymatic sensing of glucose. *Sensors and Actuators B: Chemical* 241: 349-356.
81. Huang J, Li T, Liu R, Zhang R, Wang Q, et al. (2017) Rational designed benzochalcone-based fluorescent probe for molecular imaging of hydrogen peroxide in live cells and tissues. *Sensors and Actuators B: Chemical* 248: 257-264.
82. Chen H, Lu Q, He K, Liu M, Zhang Y, et al. (2018) A cyclic signal amplification strategy to fluorescence and colorimetric dual-readout assay for the detection of H₂O₂-related analytes and application to colorimetric logic gate. *260: 908-917.*
83. Wang J, Dong J (2020) *Optical Waveguides and Integrated Optical Devices for Medical Diagnosis, Health Monitoring and Light Therapies. Sensors* 20(14): 3981.
84. Zhou Y, Ma Z (2017) Fluorescent and colorimetric dual detection of mercury (II) by H₂O₂ oxidation of o-phenylenediamine using Pt nanoparticles as the catalyst. *Sensors and Actuators B: Chemical* 249: 53-58.
85. Yang F, Jiang X, Zhong X, Wei S, Yuan R (2018) Highly sensitive electrochemiluminescence detection of mucin1 based on V2O5 nanospheres as peroxidase mimetics to catalyze H₂O₂ for signal amplification. *Sensors and Actuators B: Chemical* 265: 126-133.
86. Li N, Huang J, Wang Q, Gu Y, Wang P (2018) A reaction based one- and two-photon fluorescent probe for selective imaging H₂O₂ in living cells and tissues. *Sensors and Actuators B: Chemical* 254: 411-416.
87. Zhu B, Wu L, Wang Y, Zhang M, Zhao Z, et al. (2018) A highly selective and ultrasensitive ratiometric far-red fluorescent probe for imaging endogenous peroxynitrite in living cells. *Sensors and Actuators B: Chemical* 259: 797-802.
88. Garreffi BP, Guo M, Tokranova N, Cady NC, Castracane J, et al. (2018) Highly sensitive and selective fluorescence sensor based on nanoporous silicon-quinoline composite for trace detection of hydrogen peroxide vapors. *Sensors and Actuators B: Chemical* 276: 466-471.
89. Lyu ZM, Zhou XL, Wang XN, Li P, Xu L, et al. (2019) Miniaturized electrochemiluminescent biochip prepared

- on gold nanoparticles-loaded mesoporous silica film for visual detection of hydrogen peroxide released from living cells. *Sensors and Actuators B: Chemical* 284: 437-443.
90. Riaz MA, Yuan Z, Mahmood A, Liu F, Sui X, et al. (2020) Hierarchically porous carbon nanofibers embedded with cobalt nanoparticles for efficient H₂O₂ detection on multiple sensor platforms. *Sensors and Actuators B: Chemical* 319: 128243.
 91. Ensafi AA, Rezaloo F, Rezaei B (2016) Electrochemical sensor based on porous silicon/silver nanocomposite for the determination of hydrogen peroxide. *Sensors and Actuators B: Chemical* 231: 239-244.
 92. Hardan ANH, Azmi M (2018) *Sensors* 18: 71.
 93. Zhang MR, Chen XQ, Pan GB (2017) Electrosynthesis of gold nanoparticles/porous GaN electrode for non-enzymatic hydrogen peroxide detection. *Sensors and Actuators B: Chemical* 240: 142-147.
 94. Gong C, Shen Y, Chen J, Song Y, Chen S, et al. (2017) Microperoxidase-11@PCN-333 (Al)/three-dimensional macroporous carbon electrode for sensing hydrogen peroxide. *Sensors and Actuators B: Chemical* 239: 890-897.
 95. Cao GS, Wang P, Li X, Wang Y, Wang G, et al. (2015) A sensitive nonenzymatic hydrogen peroxide sensor based on Fe₃O₄-Fe₂O₃ nanocomposites. *Bull Mater Sci* 38: 163-167.
 96. Hua MY, Chen CJ, Chen HC, Tsai RY, Cheng W, et al. (2011) Preparation of a Porous Composite Film for the Fabrication of a Hydrogen Peroxide Sensor. *Sensors* 11(6): 5873-5885.
 97. Gupta R, Singh P, Ganesan V, Koch B, Rastogi PK, et al. (2018) Palladium nanoparticles supported on mesoporous silica microspheres for enzyme-free amperometric detection of H₂O₂ released from living cells. *Sensors and Actuators B: Chemical* 276(10): 517-525.
 98. Li Y, Weng Y, Lu S, Xue M, Yao B, et al. (2020) One-Step Hydrothermal Synthesis of N, Fe-Codoped Carbon Dots as Mimic Peroxidase and Application on Hydrogen Peroxide and Glucose Detection. *Hindawi J Nanomaterials* pp: 1-11.
 99. Peng C, Zhou S, Zhang X, Zeng T, Zhang W, et al. (2018) One pot synthesis of nitrogen-doped hollow carbon spheres with improved electrocatalytic properties for sensitive H₂O₂ sensing in human serum. *Sensors and Actuators B: Chemical* 270(1): 530-537.
 100. Ledo A, Fernandes E, Brett CMA, Barbosa RM (2020) Enhanced selectivity and stability of ruthenium purple-modified carbon fiber microelectrodes for detection of hydrogen peroxide in brain tissue. *Sensors and Actuators B: Chemical* 311: 127899.
 101. Lee DJ, Choi SW, Byun YT (2018) Room temperature monitoring of hydrogen peroxide vapor using platinum nanoparticles-decorated single-walled carbon nanotube networks. *Sensors and Actuators B: Chemical* 256: 744750.
 102. Anojci J, Guzsvány V, Vajdle O, Madarász D, Rónavári A, et al. (2016) Hydrodynamic chronoamperometric determination of hydrogen peroxide using carbon paste electrodes coated by multiwalled carbon nanotubes decorated with MnO₂ or Pt particles. *Sensors and Actuators B: Chemical* 233: 83-92.
 103. Bracamonte MV, Melchionna M, Giuliani A, Nasi L, Tavagnacco C, et al. (2017) H₂O₂ sensing enhancement by mutual integration of single walled carbon nanohorns with metal oxide catalysts: The CeO₂ case. *Sensors and Actuators B: Chemical* 239: 923-932.
 104. Bui MPN, Pham XH, Han KN, Li CA, Kim YS, et al. (2010) Electrocatalytic reduction of hydrogen peroxide by silver particles patterned on single-walled carbon nanotubes. *Sensors and Actuators B: Chemical* 150(1): 436-441.
 105. Aroutiounian VMJ (2015) Gas sensors based on functionalized carbon nanotubes. *Contemp Phys (Arm Acad Sci)* 50: 333-354.
 106. Aroutiounian VM, Adamyan AZ, Khachatryan EA, Adamyan ZN, Hernadi K, et al. (2013) *Sensors and Actuators B: Chemical* 177: 308-315.
 107. Aroutiounian V, Adamyan Z, Sayunts A, Khachatryan E, Adamyan A, et al. (2014) *Int J of Emerging Trends in Science and Technology* 1(8): 1309.
 108. Aroutiounian VM (2015) Metal Oxide Gas Sensors Decorated With Carbonnanotubes. *Lithuanian J Physics* 55(4): 319-329.
 109. Adamyan ZN, Sayunts A, Khachatryan EA, Aroutiounian VM (2017) Tin Oxide/Carbon Nanotube Nanocomposite Sensors for Some Toxic VOCs Detection. *South Florida J Development* 2(1): 1067-1093.
 110. Adamyan ZN, Sayunts A, Aroutiounian V, Khachatryan E, Adamyan A, et al. (2017) Study of Propylene Glycol, Dimethylformamide and

- Formaldehyde Vapors Sensors Based on MWCNTs/SnO₂ Nanocomposites. *Sensors & Transducers* 213(6): 38-45.
111. Adamyan Z, Sayunts, Aroutiounian V, Khachatryan E, Vrnata M, et al. (2018) Nanocomposite sensors of propylene glycol, dimethylformamide and formaldehyde vapors. *J Sens Sens Syst* 7(1): 31-41.
 112. Aroutiounian VM, Arakelyan VM, Aleksanyan M, Sayunts A, Shahnazaryan G, et al. (2017) Nanostructured Sensors for Detection of Hydrogen Peroxide Vapours. *Sensors & Transducers* 213(6): 46-53.
 113. Aroutiounian VM (2021) Gas and Biosensors Made from Metal Oxides Doped with Carbon Nanotubes. *Phys Sci & Biophys J* 5(1): 1-16.
 114. Aroutiounian VM (2020) Microelectronic Gas sensors for Non-invasive Analysis of Exhaled Gases. *J Nanomed Nanotechnol* 11(3): 1-7.
 115. Aroutiounian VM (2020) *Medicine in Armenia*. LX, pp: 118.
 116. Paredi P, Kharitonov SA, Barnes PJ (2000) Elevation of Exhaled Ethane Concentration in Asthma. *Am J Respir Crit Care Med* 162(4): 1450-1454.
 117. Kischkel S, Miekisch W, Straker EM, Sawacki A, Trefz P, et al. (2010) Breath biomarkers for lung cancer detection and assessment of smoking related effects-confounding variables, influence of normalization and statistical algorithms. *Clin Chim Acta* 411(21-22): 1637-1644.
 118. de Gennaro G, Dragonieri S, Longobardi F, Musti M, Stallone G, et al. (2010) Chemical characterization of exhaled breath to differentiate between patients with malignant pleural mesothelioma from subjects with similar professional asbestos exposure. *Anal Bioanal Chem* 398(7-8): 3043-3050.
 119. Barker M, Hengst M, Schmid J, Buers HJ, Mittermaier B, et al. (2006) Volatile organic compounds in the exhaled breath of young patients with cystic fibrosis. *Eur Respir J* 27(5): 929-936.
 120. Alkhouri N, Cikach F, Eng K, Moses J, Patel N, et al. (2014) Analysis of breath volatile organic compounds as a noninvasive tool to diagnose nonalcoholic fatty liver disease in children. *Eur J Gastroenterol Hepatol* 26(1): 82-87.
 121. Hyslop PA, Sklar LA (1984) A quantitative fluorimetric assay for the determination of oxidant production by polymorphonuclear leukocytes: its use in the simultaneous fluorimetric assay of cellular activation processes. *Anal Biochem* 141(1): 280-286.
 122. Broza YY, Haick H (2013) Nanomaterial-based sensors for detection of disease by volatile organic compounds. *Nano medicine* 8(5): 785-806.
 123. Jobsis Q, Raatgeep HC, Schellekens SL, Hop WC, Hermans PW, et al. (1998) Hydrogen peroxide in exhaled air of healthy children: reference values. *Eur Respir J* 12(2): 483-485.
 124. Scheideler L, Manke HG, Schwulera U, Inacker O, Hämmerle H (1993) Detection of Nonvolatile Macromolecules in Breath: A Possible Diagnostic Tool?. *Am Rev Respir Dis* 148(3): 778-784.
 125. Tonnel AB, Wallaert B (1990) Oxidants and bronchial inflammatory processes. *Eur Respir J* 3(9): 987-988.
 126. Cluzel M, Damon M, Chanez P, Bousquet J, Crastes de Paulet A, et al. (1987) Enhanced alveolar cell luminol-dependent chemiluminescence in asthma. *Allergy Clin Immunol* 80(2): 195-201.
 127. Nowak D, Antczak A, Krol M, Pietras T, Shariati B, et al. (1996) Increased content of hydrogen peroxide in the expired breath of cigarette smokers. *Eur Respir J* 9(4): 652-657.
 128. Baldwin SR, Grum CM, Simon RH, Ketani LH, Boxer LA, et al. (1986) Oxidant activity in expired breath of patients with adult respiratory distress syndrome. *Lancet* 1(8471): 1-4.
 129. Muller M, Burchardi H, Kietzmann D, Kahl R, Kettler D (1993) Hydrogen peroxide in expired breath condensate of patients with acute respiratory failure and with ARDS. *Intensive Care Med* 19(2): 78-81.
 130. Sznajder JJ, Fraiman A, Hall JB, Nahum A, Factor P, et al. (1989) Increased Hydrogen Peroxide in the Expired Breath of Patients with Acute Hypoxemic Respiratory Failure. *Chest* 96(3): 606-612.
 131. Jobsis Q, Raatgeep HC, de Jongste JC, Hermans PWM (1997) Hydrogen peroxide in exhaled air is increased in stable asthmatic children. *Eur Respir J* 10(3): 519-521.
 132. Moller W, Heimbeck I, Weber N, Saba GK, Korner B, et al. (2010) *J Aerosol Med Pulmon Drug Deliv* 23(3): 129-135.
 133. Repine JE, Bast A, Lankhorst I (1997) Oxidative stress in chronic obstructive pulmonary disease. Oxidative Stress Study Group. *Am J Respir Crit Care Med* 156(2): 341-357.

134. Rahman I, Adcock IM (2006) Oxidative stress and redox regulation of lung inflammation in COPD. *Eur Respir J* 28(1): 219-242.
135. Dekhuijzen P, Aben K, Dekker I, Aarts LP, Wielders PL, et al. (1996) Increased exhalation of hydrogen peroxide in patients with stable and unstable chronic obstructive pulmonary disease. *Am J Respir Crit Care Med* 154(3): 813-816.
136. van Beurden WJ, Dekhuijzen PN, Harff GA, Smeenk FWJM (2002) Variability of Exhaled Hydrogen Peroxide in Stable COPD Patients and Matched Healthy Controls. *Respiration* 69(3): 211-216.
137. Haugen TS, Skjonsberg OH, Kahler H, Lyberg T (1999) Production of oxidants in alveolar macrophages and blood leukocytes. *Eur Respir J* 14(5): 1100-1105.
138. Nowak D, Kasielski M, Antczak A, Pietras T, Bialasiewicz P (1999) Increased content of thiobarbituric acid-reactive substances and hydrogen peroxide in the expired breath condensate of patients with stable chronic obstructive pulmonary disease: no significant effect of cigarette smoking. *Respir Med.* 93(6): 389-396.
139. Kostikas K, Papatheodorou G, Psathakis K, Panagou P, Loukides S, et al. (2003) Oxidative stress in expired breath condensate of patients with COPD. *Chest* 124(4): 1373-1380.
140. Winkler-Heil R, Hofmann W (2002) *Ann Occup Hyg* 46: S326.
141. Balashazy I, Hofmann W, Heistracher T (2003) Local particle deposition patterns may play a key role in the development of lung cancer. *J Appl Physics* 94(5): 1719-1725.
142. Möller W, Häussinger K, Winkler-Heil R, Stahlhofen W, Meyer T, et al. (2004) Mucociliary and long-term particle clearance in the airways of healthy nonsmoker subjects. *J Appl Physics* 97: 2200-2206.
143. Möller W, Felten K, Sommerer K, Scheuch G, Meyer G, et al. (2008) Deposition, retention, and translocation of ultrafine particles from the central airways and lung periphery. *Am J Respir Crit Care Med* 177(4): 426-432.
144. Isik B, Ceylan A, Isik R (2007) Oxidative stress in smokers and non-smokers. *Inhal Toxicol* 19(9): 767-769.
145. Nagaraja C, Shashibhushan BL, Sagar, Asif M, Manjunath PH (2012) Hydrogen peroxide in exhaled breath condensate: A clinical study. *Lung India* 29(2): 123-127.
146. Soyer OU, Dizdar EA (2006) *Allergy* 61: 16.
147. Loukides S, Horvath I (1998) *Am J Respir Crit Care Me* 158: 99.
148. Mutlu GM, Garey KW, Robbins RA, Danziger LH, Rubinstein I (2001) Collection and analysis of exhaled breath condensate in humans. *Am J Respir Crit Care Med* 164(5): 731-737.
149. Van Hoydonck PG, Wuyts WA, Vanaudenaerde BM, Schouten EG, Dupont LJ, et al. (2004) Quantitative analysis of 8-isoprostane and hydrogen peroxide in exhaled breath condensate. *Eur Respir J* 23(2): 189-192.
150. Haugen TS, Skjonsberg OH, Kähler H, Lyberg T (1999) Production of oxidants in alveolar macrophages and blood leukocytes. *Eur Respir J* 14(5): 1100-1105.
151. Stefanska J, Sokolowska M, Sarniak A, Włodarczyk A, Doniec Z, et al. (2010) Apocynin decreases hydrogen peroxide and nitrate concentrations in exhaled breath in healthy subjects. *Pulmon Pharm Therapeutics* 23(1): 48-54.
152. Montuschi P (2003) *Eur Respir J* 21: 433.
153. Rutgers SR, Timens W, Kaufmann HF, van der Mark TW, Koëter GH, et al. (2000) Comparison of induced sputum with bronchial wash, bronchoalveolar lavage and bronchial biopsies in COPD. *Eur Respir J* 15(1): 109-115.
154. Montuschi P (2007) Review: Analysis of exhaled breath condensate in respiratory medicine: methodological aspects and potential clinical applications. *Therapeutic Advances in Respiratory Disease* 1(1): 5-23.
155. Hoffmeyer F, Harth V (2007) *J Physiol Pharmacol* 58: 289.
156. Borrill ZL, Roy K, Singh D (2008) Exhaled breath condensate biomarkers in COPD. *Eur Respir J* 32: 472-486.
157. Kostikas K, Gaga M, Papatheodorou G, Karamanis T, Orphanidou D, et al. (2005) Leukotriene B4 in exhaled breath condensate and sputum supernatant in patients with COPD and asthma. *Chest* 127(5): 1553-1559.
158. Garey KW, Nenhauser MM, Robbins RA, Danziger LH, Rubinstein I (2004) Markers of Inflammation in Exhaled Breath Condensate of Young Healthy Smokers. *Am J Respir Crit Care Med* 170(1): 22-26.
159. Loukides S, Koutsokera A, Gourgoulisanis KI, Kostikas

- K (2008) Biomarkers in the exhaled breath condensate of healthy adults: mapping the path towards reference values. *Curr Med Chem* 15(6): 620-630.
160. Kasielski M, Nowak D (2001) Long-term administration of N-acetylcysteine decreases hydrogen peroxide exhalation in subjects with chronic obstructive pulmonary disease. *Respir Med* 95(6): 448-456.
161. van Beurden WJC, Harff GA, Dekhuijzen PNR, van der Poel-Smet SM, Smeenk FWJM (2003) Effects of Inhaled Corticosteroids with Different Lung Deposition on Exhaled Hydrogen Peroxide in Stable COPD Patients. *Respiration* 70(3): 242-248.
162. Kostikas K, Papatheodorou G, Ganas K, Psathakis K, Panagou P, et al. (2002) pH in expired breath condensate of patients with inflammatory airway diseases. *Am J Respir Crit Care Med* 165(10):1364-1370.
163. Ferris BG (1978) Epidemiology Standardization Project (American Thoracic Society). *Am Rev Respir Dis* 118(6 Pt 2): 1-120.
164. Quanjer PH, Tammeling G, Cotes JE, Pedersen OF, Peslin R, et al. (1993) Lung volumes and forced ventilatory flows. Report Working Party Standardization of Lung Function Tests, European Community for Steel and Coal. Official Statement of the European Respiratory Society. *Eur Respir J* 16: 5-40.
165. Peng G, Hakim M, Broza YY, Billan S, Abdah-Bortnyak R, et al. (2010) Detection of lung, breast, colorectal, and prostate cancers from exhaled breath using a single array of nanosensors. *Br J Cancer* 103: 542-551.
166. Nakhleh MK, Amal H, Jeries R, Broza YY, Aboud M, et al. (2017) Diagnosis and Classification of 17 Diseases from 1404 Subjects via Pattern Analysis of Exhaled Molecules. *ACS Nano* 11(1): 112-125.
167. Hashoul D, Haick H (2019) Sensors for detecting pulmonary diseases from exhaled breath. *Eur Respir Rev* 28: 190011.
168. Velusamy V, Palanisamy S, Chen SM, Chen TW, Selvam S, et al. (2017) Graphene dispersed cellulose microfibrils composite for efficient immobilization of hemoglobin and selective biosensor for detection of hydrogen peroxide. *Sens Actuators B* 252: 175-182.
169. Gasparri R, Sedda G, Spaggiari L (2018) The Electronic Nose's Emerging Role in Respiratory Medicine. *Sensors* 18(9): 3029.
170. Wilson AD, Baietto M (2011) Advances in Electronic-Nose Technologies Developed for Biomedical Applications. *Sensors* 11(1): 1105.
171. Dragonieri S, Pennazza G, Carratu P, Resta Lung O (2017) Electronic Nose Technology in Respiratory Diseases. *Lung* 195: 157-165.
172. Montuschi P, Mores N, Trové A, Mondino C, Barnes PJ (2013) The Electronic Nose in Respiratory Medicine. *Respiration* 85: 72-84.
173. Bikov A, Lazar Z, Horvath IJ (2015) Established methodological issues in electronic nose research: how far are we from using these instruments in clinical settings of breath analysis?. *J Breath Res* 9: 034001.
174. D'Amico A, Pennazza G, Santonico M, Martinellia E, Roscioni C, et al. (2010) An investigation on electronic nose diagnosis of lung cancer. *Lung Cancer* 68(2): 170-176.
175. Mazzone PJ, Wang XF, Xu Y, Mekhail T, Beukemann MC, et al. (2012) Exhaled Breath Analysis with a Colorimetric Sensor Array for the Identification and Characterization of Lung Cancer. *J Thorac Oncol* 7: 137-142.
176. Shlomi D, Abud M (2017) *Ibid* 12: 1544.
177. Fens N, Roldaan AC, van der Schee MP, Zwinderman AH (2011) External validation of exhaled breath profiling using an electronic nose in the discrimination of asthma with fixed airways obstruction and chronic obstructive pulmonary disease. *Clin Exp Allergy* 41(10): 1371-1378.
178. Hattesoehl ADM, Jorres RA, Dressel H, Schmid S, Vogelmeier C, et al. (2011) Discrimination between COPD patients with and without alpha 1-antitrypsin deficiency using an electronic nose. *Respirology* 16(8): 1258-1264.
179. Dragonieri S, Annema JT, Schot R, van der Schee MPC, Spanevello A, et al. (2009) An electronic nose in the discrimination of patients with non-small cell lung cancer and COPD. *Lung Cancer* 64(2): 166-170.
180. Montuschi P, Santonico M, Mondino C, Pennazza G, Mantini BEng G, et al. (2010) Diagnostic Performance of an Electronic Nose, Fractional Exhaled Nitric Oxide, and Lung Function Testing in Asthma. *Chest* 137(4): 790-796.
181. Plaza V, Crespo A, Giner J, Merino JL, Ramos-Barbón D, et al. (2015) Inflammatory Asthma Phenotype Discrimination Using an Electronic Nose Breath Analyzer. *J Invest Allergol Clin Immunol* 25(6): 431-437.
182. de Vries R, Brinkman P, van der Schee MP, Fens

- N, Dijkers E, et al. (2015) Integration of electronic nose technology with spirometry: validation of a new approach for exhaled breath analysis. *J Breath Res* 9: 046001.
183. Greulich T, Hattesoehl A (2013) *Eur Respir J* 42: 145-155.
184. Dragonieri S, Porcelli F, Longobardi F, Carratù P, Aliani M, et al. (2015) An electronic nose in the discrimination of obese patients with and without obstructive sleep apnoea. *J Breath Res* 9: 026005.
185. Joensen O, Paff T, Haarman EG, Ib Skovgaard M, Jensen PO, et al. (2014) Exhaled Breath Analysis Using Electronic Nose in Cystic Fibrosis and Primary Ciliary Dyskinesia Patients with Chronic Pulmonary Infections. *PLoS One* 9: 115584.
186. Bruins M, Rahim Z, Bos A, Endtzbc H, Belkumb A, et al. (2013) Diagnosis of active tuberculosis by e-nose analysis of exhaled air. *Tuberculosis* 93(2): 232-238.
187. Yang HY, Peng HY, Chang CH, Chen PC (2017) Diagnostic accuracy of breath tests for pneumoconiosis using an electronic nose. *J Breath Res* 12: 016001.
188. Wilson AD (2018) Application of Electronic-Nose Technologies and VOC-Biomarkers for the Noninvasive Early Diagnosis of Gastrointestinal Diseases. *Sensors* 18(8): 2613.
189. Scarlata S, Pennazza G, Santonico M, Santangelo S, Bartoli IR, et al. (2017) Screening of Obstructive Sleep Apnea Syndrome by Electronic-Nose Analysis of Volatile Organic Compounds. *Sci Rep* 7: 11938.
190. McWilliams A, Beigi P, Srinidhi A, Lam S, MacAulay CE (2015) Sex and Smoking Status Effects on the Early Detection of Early Lung Cancer in High-Risk Smokers Using an Electronic Nose. *IEEE Trans Biomed Eng* 62(8): 2044-2054.
191. Aroutiounian VM (2021) On Non-Invasive Measurements of Exhaled Aceton Using Metal Oxide Nanosensors. *J Nanomedicine & Nanotechnology* 12(2): 560.
192. Aroutiounian VM (2021) Non-Invasive Metal Oxide Sensors on Exhaled Aceton. *J Contemp Phys (Arm Acad Sci)* 56: 117-132.
193. Aroutiounian VM, Hovhannisyan A (2020) *Biomed J Sci & Tech Res* 27: 20422.

